Micro-mechanics and data-driven based reduced order models for multi-scale analyses of woven composites

Ling Wu[a,], Laurent Adam[b], Ludovic Noels[a]

[a] *University of Liege, Department of Aeronautics and Mechanical Engineering, Computational & Multiscale Mechanics of Materials, Allée de la découverte 9, B-4000 Liège, Belgium*

[b] *MSC Software Belgium SA (e-Xstream engineering) Rue Emile Francqui B9, B-1435 Mont-Saint-Guibert Belgium*

Abstract

Order reduction of woven composite materials is based on the definition of short fibres reinforced matrix material pseudo-grains completed by pure matrix parts. The former ones model the curved yarns, which are assimilated to continuous fibre reinforced matrix materials, in woven composites, and the latter ones model the matrix response. The homogenisation is achieved by recursively using micro-mechanics models, such as mean-field homogenisation and Voigt's rule of mixture, and on the laminate theory.

The pseudo-grains number and micro-structural features such as orientation, aspect ratio and volume fraction are considered as the Reduced Order Model (ROM) parameters and are identified following the approach of Deep Material Network (DMN): a set of homogenised elasticity tensors evaluated by computational homogenisation of woven unit-cells is used as training data in order to identify the topological parameters of the ROM. Once the topological parameters are identified, the proposed ROM can be used to conduct nonlinear analyses of woven composites.

The accuracy and efficiency of the proposed ROM have been verified by comparing the predictions with direct numerical simulations on two different woven unit cells.

Keywords: Reduced Order Model, Deep-Material Network, Woven Composites, Data-Driven, Homogenisation

1. Introduction

Woven composites are widely used as structural components in aerospace, automotive, marine, civil, or sporting industries due to their excellent mechanical properties, particularly high stiffness and strength to weight ratio [1]. They

Email addresses: l.wu@ulg.ac.be (Ling Wu), laurent.adam@Hexagon.com (Laurent Adam), l.noels@ulg.ac.be (Ludovic Noels)

serve as a suitable alternative to unidirectional laminates because of their lower production costs, improved out-of-plane properties and good impact resistance. However, their architected textile reinforcements increase the analysis complexity significantly from the design perspective.

As typical heterogeneous materials, woven composites have various mechanical behaviours at the micro-, meso- and macro-scales. UD-fibre reinforced matrix can be seen in yarns at the micro-scale, with the diameter of each fibre constituting the yarns being of around a few micrometers for carbon, and a few to tens of micrometers for glass fibres. At the meso-scale with dimensions of several to tens of millimetres, yarns, each of whose includes several thousands of fibres (e.g. 3000 to 12000 [2]), are woven following standard weaves, e.g. plain, satin and twill, to form the reinforcements of the composite material. Finally, at the final macro-scale, which refers to the component level with dimensions of the order of some centimetres to several meters, the material has a laminate structure. Although macro-scale mechanical models have been proposed [3–5], in which the textile reinforcement is considered as an anisotropic continuum, strictly speaking, the material is homogeneous only at the microscopic level because of the possible relative sliding between yarns at the meso-scopic level. Consequently, the modelling of woven composites should encompasses the different scales, which remains challenging because of the difficulty in defining a widely accepted model which can describe accurately the mechanical behaviours at the fibre, yarn and woven scales.

Computational homogenisation, as a versatile tool, can be applied on the numerical analysis of a wide range of heterogeneous materials [6, 7]. Using the periodic character of woven composites, computational homogenisation can theoretically be applied on a representative unit cell. However the direct finite element analysis with micro-scale details, including the fibre representation within the yarns, on a meso-scale unit cell is not realistic. Besides, using a two-step computational homogenisation in order to capture the non-linear yarn response from computational homogenisation of the UD fibre Representative Volume Element (RVE) is not practical for woven composites either. Indeed a nonlinear analysis of a meso-scale unit cell with a detailed 3D yarn structure itself is already computationally expensive, not to mention the cost of the micro-scale computational homogenisation at each Gauss point of the yarns. Therefore, most of the numerical works on woven composites focus on woven unit cells described at the meso-scale, which is seen as the key scale for woven composites, by treating the yarn as a homogeneous material [8–12].

In the non-linear range, multi-scale analyses linking the meso- and macro-scales are still not affordable with computational multi-scale methods because of their inherent computational cost. In order to reduce the computational cost and make the coupling of scales become possible, analytical or semi-analytical methods are widely adopted. The asymptotic analysis [13] is performed at the component level in [14], and is combined with a reduced order model of the unit woven volume element. The micro-mechanics self-consistent [15] method is applied in [16] with piece-wise phase fields defined by a strain clustering process also based on direct numerical simulations of woven unit cell. In this

reference, the yarns are treated as homogeneous elastic materials whose properties are pre-computed by computational homogenisation. Another way of using micro-mechanical models to represent the woven response is to represent the yarns as a collections of ellipsoids and applying a Mori-Tanaka-based Mean-Field-Homogenisation (MFH) [17], as suggested in [11] in the context of elastic damage. The accuracy of this approach remains however limited for elasto-plasticity. Computational homogenisation efficiency can also be improved by conducting off-line simulations in order, either to build surrogate models of the inelastic response of the RVE, e.g. using artificial neural-networks [18, 19], or to construct a synthetic data base of homogenised responses [20] that can further be used in data-driven and model-free analyses [21, 22]. However, both the training of RNN and creation of a data base require a large number of direct numerical simulations of the RVE or unit cell (or a large number of experiments), which is achievable for UD composites but is more computationally intense in the case of woven composites. Reduced Order Models (ROMs) can then be used directly in multi-scale simulations, but also to construct the off-line simulation data base needed for data-driven macro-scale analyses [23].

Recently, a deep material network method was proposed in [24] and was subsequently applied on the analysis of woven composites at both the micro- and meso-scales in [25]. This latter homogenisation method incorporates analytical homogenisation solutions into a neural network model yielding mechanistic building blocks, the RNN being trained considering only elastic data of RVE simulations, see also the theoretical analysis in [26] and the implementation details in [27]. Taking advantage of this data-driven concept and inspired by the successful modelling of random short fibre reinforced matrix material using Voigt's rule of mixtures [28, 29] and MFH [30], in order to reduce the computation cost of woven composites, and to preserve at the same time as much as possible the micro- and meso-structural information, micro-mechanics based approximate models are proposed in this paper. The computational inexpensive mechanics models such as Voigt's rule of mixtures, MFH and laminate theory, can be totally or partially combined to reproduce the nonlinear response of woven composites. Depending on the adopted basic mechanics models and on their applied ordering, three ROMs are proposed as illustrated in Fig. 1.

The yarn of woven composites is made of a continuous fibre reinforced matrix material. Because the fibre orientation of a yarn varies in a woven unit cell, in the proposed ROMs, the yarn is modelled as a set of discontinuous but straight fibres like short fibre reinforced matrix.

- The first or "Voigt-Mori-Tanaka" scheme is denoted by "V-M" and is illustrated in Fig. 1(b). In this scheme, the woven composite unit cell is treated as an aggregate of pseudo-grains. Beside one pure matrix pseudo-grain, the other pseudo-grains correspond to short fibre reinforced matrix materials with different fibre orientations and aspect ratios.

- The second one or "Laminate-Voigt-Mori-Tanaka" scheme is denoted by "LVM" and is illustrated in Fig. 1(c). Compared to the "V-M" scheme, instead of treating the pure matrix as a pseudo-grain, the second scheme

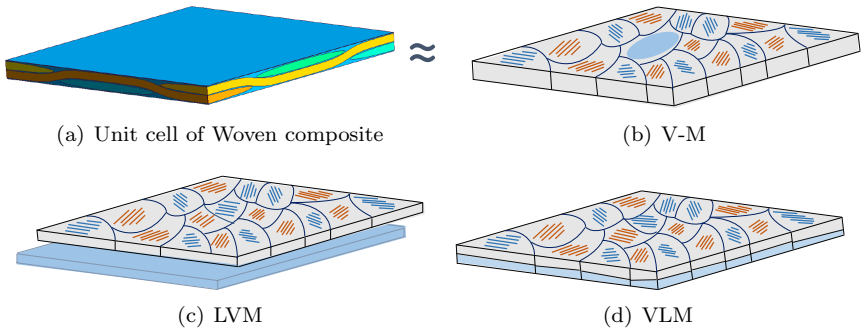

(a) Unit cell of Woven composite (b) V-M

(c) LVM (d) VLM

Figure 1: Woven composites approximation: (a) A woven unit cell is successively approximated (b) by an aggregate of pseudo-grains of short fibre reinforced matrix and of pure matrix (V-M); or (c) by a laminate of two plies respectively made of a pure matrix and of an aggregate of pseudo-grains of short fibre reinforced matrix (LVM); or again (d) by an aggregate of pseudo-grains of 2-ply laminates made of short fibre reinforced matrix and of pure matrix (VLM).

models the woven composite unit cell as a laminate with one pure matrix ply and a ply of an aggregate of short fibre reinforced matrix pseudo-grains.

- The last or "Voigt-Laminate-Mori-Tanaka" scheme is denoted by "VLM" and is illustrated in Fig. 1(d). The "VLM" scheme also treats the woven composite unit cell as an aggregate of pseudo-grains, and each pseudo-grain is a laminate which has one pure matrix ply and a short fibre reinforced matrix ply.

The accuracy of these proposed ROMs relies on a series of topology parameters corresponding to the studied woven unit cell. These parameters include pseudo-grain volume fractions and orientations, short fibre aspect ratios etc. They are abstract descriptions of the material structure at the meso-scale. The concept of data-driven approaches can be used to optimise the topology parameters definition of each of the ROM by considering elastic full-field simulations of the woven unit cell. Although plain woven composite material is used as a detailed example of application, the proposed method is not limited to this weaving pattern.

Organisation of the paper is as follows. In Section 2, the basic micro-mechanics models that will be used to build the three ROMs are summarised. Section 3 presents the three developed ROMs and their parametrised elasticity tensors. The training of these three models, i.e. the optimisation loop allowing to define the parameters of the ROMs, from direct numerical estimations of the homogenised elasticity tensor is explained in Section 4. Once the parameters are defined, the online resolution of the ROM is detailed in the nonlinear range in Section 5. The methodology is then applied on plain woven unit cells in Section 6. Finally conclusions are drawn.

2. Basic mechanical models in linear elastic case

Since the topology parameters of the proposed ROMs will be sought out from the linear elastic response of unit woven cells, in this section, the main theories and conclusions of Mean-Filed-Homogenisation (MFH), Voigt's rule of mixtures and laminate theories are recalled briefly for linear elastic materials.

2.1. Mean-field homogenisation for short fibre-reinforced matrix

Mean-field homogenisation (MFH) is applied to compute the mechanical properties of the short fibre reinforced matrix. The Mori-Tanaka [17] inclusion interaction assumption is adopted, because of its good accuracy in the modelling of inclusion reinforced matrix material [31]. In all the proposed schemes, i.e. the "V-M", "LVM" and "VLM" schemes, the continuous fibre reinforced yarn is modelled by several pseudo-grains of short fibre reinforced matrix material, which have their own unique fibre orientations and aspect ratios. For the consistency of notation, we use the subscript "i" for the homogenised elasticity tensor and related parameters of each short fibre reinforced matrix pseudo-grain, and $i = 1, ..., N_\mathrm{s}$ with the total number of them being N_s.

The fibre volume fraction in each short fibre composite model is assumed to be consistent with the fibre volume fraction in the yarns denoted by V_I[1]. The matrix phase is modelled as an isotropic material, and the fibre phase as a transverse isotropic material. The following tensor expressions are expressed in the principal coordinates of the fibre. The homogenised elasticity tensor is computed using the MFH theory and reads

$$\mathbb{C}_i = [V_\mathrm{I}\mathbb{C}_\mathrm{I} : \mathbb{B}_i^\epsilon + (1 - V_\mathrm{I})\mathbb{C}_0] : [V_\mathrm{I}\mathbb{B}_i^\epsilon + (1 - V_\mathrm{I})\mathbb{I}]^{-1} , \tag{1}$$

where $\mathbb{C}_\mathrm{I}$ and $\mathbb{C}_0$ are respectively the elasticity tensors of fibre and matrix, and $\mathbb{I}$ is the fourth order identity tensor. The strain concentration tensor $\mathbb{B}_i^\epsilon$ of the pseudo-grain i reads, according to the M-T assumption,

$$\mathbb{B}_i^\epsilon(\mathrm{I}_i, \mathbb{C}_0, \mathbb{C}_\mathrm{I}) = \{\mathbb{I} + \mathbb{S}(\mathrm{I}_i, \mathbb{C}_0) : [(\mathbb{C}_0)^{-1} : \mathbb{C}_\mathrm{I} - \mathbb{I}]\}^{-1} , \tag{2}$$

where the Eshelby tensor [33], $\mathbb{S}(\mathrm{I}_i, \mathbb{C}_0)$, depends on the elasticity tensor of the matrix phase $\mathbb{C}_0$ and on "I_i", the geometry of the inclusions in the pseudo-grain i, which are short fibres and can be simplified as prolate ellipsoidal inclusions. Therefore "I_i" is parametrised by the inclusion's aspect ratio α_i. The detailed expression of $\mathbb{S}$ is given in Appendix A. Because all the short fibre reinforced matrix pseudo-grains have the same elasticity tensors of fibre $\mathbb{C}_\mathrm{I}$ and matrix $\mathbb{C}_0$, and because we assume that the fibre volume fraction $V_\mathrm{I} = V_\mathrm{I}^\mathrm{yarn}$ is uniform, their homogenised elasticity tensor is denoted by $\mathbb{C}_i(\alpha_i)$ to indicate the difference. It has to be noted that these homogenised elasticity tensors are expressed with respect to the principal coordinates of the fibres.

[1] It is worth noting that the fibre volume fraction in the yarns V_I can also be considered as a variable if the variation of V_I in the yarns is considered [32]. Using a variable V_I in the proposed models is straightforward.

2.2. Voigt's rule of mixtures

Voigt's rule of mixtures [29] is adopted to evaluate the mechanical response of the aggregate of pseudo-grains. Considering an aggregate of N_{g} pseudo-grains, the volume fraction of each grain is noted by v_i and $\sum_{i=1}^{N_{\mathrm{g}}} v_i = 1.0$. According to Voigt's assumption, which states that all the grains experience the same strain, the elasticity tensor of the aggregate reads,

$$\mathbb{C}^{\mathrm{v}} = \sum_{i=1}^{N_{\mathrm{g}}} v_i \mathbb{R}^{\mathrm{T}}(\boldsymbol{\theta}_i) : \mathbb{C}_i^{\mathrm{g}} : \mathbb{R}(\boldsymbol{\theta}_i)\,, \tag{3}$$

where $\mathbb{R}(\boldsymbol{\theta}_i)$ is a rotation tensor corresponding to the angle vector $\boldsymbol{\theta}_i$, which converts the expression of $\mathbb{C}_i^{\mathrm{g}}$ from its local coordinates (i.e. the pseudo-grain principal axes) to the global ones.

2.3. Two-ply laminate

The laminate theory has been widely used for composite analyses. The homogenised elastic properties of a ply-laminate are reformulated by defining a strain concentration tensor $\mathbb{P}_{\mathrm{A}}$ in this section. First, two forth-order operator tensors $\mathbb{M}_{\mathrm{I}}$ and $\mathbb{M}_{\mathrm{o}}$ are defined respectively to collect the in-plane and out-of-plane strain and stress components. Using the notations "x-y" for the in-plane components and "z" for the out-of-plane direction, the Voigt's notations of stress and strain tensors are considered in the order $\{xx,\, yy,\, zz,\, xy,\, xz,\, yz\}$, so that the operator tensors $\mathbb{M}_{\mathrm{I}}$ and $\mathbb{M}_{\mathrm{o}}$ can be simply written in the Voigt's notations as

$$\mathbf{M}_{\mathrm{I}} = \begin{bmatrix} 1 & 0 & 0 & 0 & 0 & 0 \\ 0 & 1 & 0 & 0 & 0 & 0 \\ 0 & 0 & 0 & 0 & 0 & 0 \\ 0 & 0 & 0 & 1 & 0 & 0 \\ 0 & 0 & 0 & 0 & 0 & 0 \\ 0 & 0 & 0 & 0 & 0 & 0 \end{bmatrix}, \tag{4}$$

for the in-plane components and

$$\mathbf{M}_{\mathrm{o}} = \begin{bmatrix} 0 & 0 & 0 & 0 & 0 & 0 \\ 0 & 0 & 0 & 0 & 0 & 0 \\ 0 & 0 & 1 & 0 & 0 & 0 \\ 0 & 0 & 0 & 0 & 0 & 0 \\ 0 & 0 & 0 & 0 & 1 & 0 \\ 0 & 0 & 0 & 0 & 0 & 1 \end{bmatrix}, \tag{5}$$

for the out-plane ones. We use $\mathbb{C}_{\mathrm{A}}$ and $\mathbb{C}_{\mathrm{B}}$ respectively for the elasticity tensors of the two plies, and $\mathbb{C}_{\mathrm{L}}$ for the elasticity tensor of the laminate. The same subscripts are also used for their respective stresses and strains. The volume fraction of the two plies are respectively v_{A} and v_{B} with $v_{\mathrm{A}} + v_{\mathrm{B}} = 1.0$, and one has thus

$$\boldsymbol{\varepsilon}_{\mathrm{L}} = v_{\mathrm{A}}\boldsymbol{\varepsilon}_{\mathrm{A}} + v_{\mathrm{B}}\boldsymbol{\varepsilon}_{\mathrm{B}}\,, \quad \text{and} \quad \boldsymbol{\sigma}_{\mathrm{L}} = v_{\mathrm{A}}\boldsymbol{\sigma}_{\mathrm{A}} + v_{\mathrm{B}}\boldsymbol{\sigma}_{\mathrm{B}}\,. \tag{6}$$

Within the plane, we have

$$\mathbb{M}_{\mathrm{I}} : \boldsymbol{\varepsilon}_{\mathrm{A}} = \mathbb{M}_{\mathrm{I}} : \boldsymbol{\varepsilon}_{\mathrm{B}} = \mathbb{M}_{\mathrm{I}} : \boldsymbol{\varepsilon}_{\mathrm{L}} \,, \tag{7}$$

whilst the out-of-plane relation reads

$$\mathbb{M}_{\mathrm{o}} : \boldsymbol{\sigma}_{\mathrm{A}} = \mathbb{M}_{\mathrm{o}} : \boldsymbol{\sigma}_{\mathrm{B}} = \mathbb{M}_{\mathrm{o}} : \boldsymbol{\sigma}_{\mathrm{L}} \,. \tag{8}$$

The first equality of this last Eq. (8) successively leads to

$$\begin{aligned} \mathbb{M}_{\mathrm{o}} : \mathbb{C}_{\mathrm{A}} : \boldsymbol{\varepsilon}_{\mathrm{A}} &= \mathbb{M}_{\mathrm{o}} : \mathbb{C}_{\mathrm{B}} : \boldsymbol{\varepsilon}_{\mathrm{B}} \\ v_{\mathrm{B}} \mathbb{M}_{\mathrm{o}} : \mathbb{C}_{\mathrm{A}} : \boldsymbol{\varepsilon}_{\mathrm{A}} &= \mathbb{M}_{\mathrm{o}} : \mathbb{C}_{\mathrm{B}} : (\boldsymbol{\varepsilon}_{\mathrm{L}} - v_{\mathrm{A}} \boldsymbol{\varepsilon}_{\mathrm{A}}) \,, \end{aligned}$$

and finally,

$$\mathbb{M}_{\mathrm{o}} : [v_{\mathrm{B}} \mathbb{C}_{\mathrm{A}} + v_{\mathrm{A}} \mathbb{C}_{\mathrm{B}}] : \boldsymbol{\varepsilon}_{\mathrm{A}} = \mathbb{M}_{\mathrm{o}} : \mathbb{C}_{\mathrm{B}} : \boldsymbol{\varepsilon}_{\mathrm{L}} \,. \tag{9}$$

Finally, adding equation $\mathbb{M}_{\mathrm{I}} : \boldsymbol{\varepsilon}_{\mathrm{A}} = \mathbb{M}_{\mathrm{I}} : \boldsymbol{\varepsilon}_{\mathrm{L}}$ to the respective two sides of Eq. (9) yields

$$[\mathbb{M}_{\mathrm{o}} : (v_{\mathrm{B}} \mathbb{C}_{\mathrm{A}} + v_{\mathrm{A}} \mathbb{C}_{\mathrm{B}}) + \mathbb{M}_{\mathrm{I}}] : \boldsymbol{\varepsilon}_{\mathrm{A}} = [\mathbb{M}_{\mathrm{o}} : \mathbb{C}_{\mathrm{B}} + \mathbb{M}_{\mathrm{I}}] : \boldsymbol{\varepsilon}_{\mathrm{L}} \,. \tag{10}$$

We denote

$$\mathbb{P}_{\mathrm{A}} = \{\mathbb{M}_{\mathrm{I}} + \mathbb{M}_{\mathrm{o}} : [v_{\mathrm{B}} \mathbb{C}_{\mathrm{A}} + v_{\mathrm{A}} \mathbb{C}_{\mathrm{B}}]\}^{-1} : \{\mathbb{M}_{\mathrm{I}} + \mathbb{M}_{\mathrm{o}} : \mathbb{C}_{\mathrm{B}}\} \,, \tag{11}$$

so that

$$\boldsymbol{\varepsilon}_{\mathrm{A}} = \mathbb{P}_{\mathrm{A}} : \boldsymbol{\varepsilon}_{\mathrm{L}} \quad \text{and} \quad \boldsymbol{\varepsilon}_{\mathrm{B}} = \frac{1}{v_{\mathrm{B}}} (\mathbb{I} - v_{\mathrm{A}} \mathbb{P}_{\mathrm{A}}) : \boldsymbol{\varepsilon}_{\mathrm{L}} \,, \tag{12}$$

and

$$\begin{aligned} \boldsymbol{\sigma}_{\mathrm{L}} &= v_{\mathrm{A}} \mathbb{C}_{\mathrm{A}} : \boldsymbol{\varepsilon}_{\mathrm{A}} + v_{\mathrm{B}} \mathbb{C}_{\mathrm{B}} : \boldsymbol{\varepsilon}_{\mathrm{B}} \\ &= [v_{\mathrm{A}} \mathbb{C}_{\mathrm{A}} : \mathbb{P}_{\mathrm{A}} + \mathbb{C}_{\mathrm{B}} : (\mathbb{I} - v_{\mathrm{A}} \mathbb{P}_{\mathrm{A}})] : \boldsymbol{\varepsilon}_{\mathrm{L}} \,, \end{aligned} \tag{13}$$

which eventually leads to

$$\mathbb{C}_{\mathrm{L}} = v_{\mathrm{A}} [\mathbb{C}_{\mathrm{A}} - \mathbb{C}_{\mathrm{B}}] : \mathbb{P}_{\mathrm{A}} + \mathbb{C}_{\mathrm{B}} \,. \tag{14}$$

3. Woven unit cell elastic property estimations

In this section, three ROMs for woven composites are developed in elasticity using the basic micro-mechanics models presented in Section 2. The topology parameters corresponding to the woven unit cell structure are summarised for each of the presented model and these parameters will be identified using the parametrised elasticity tensors in the next section.

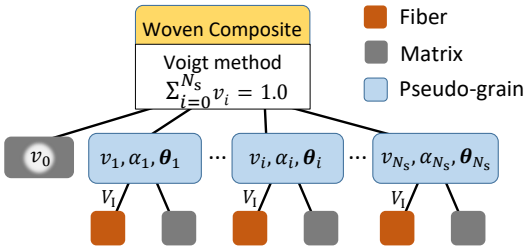

Figure 2: Computational network of the "V-M" scheme.

3.1. Voigt-MFH ("V-M") scheme

The "V-M" scheme reported in Fig. 1(b) computes the homogenised response of woven unit cells following a two-step process with the bottom to top process path illustrated in the material network of Fig. 2. Considering N_s pseudo-grains to represent the yarns, the two-step process follows

- Firstly, the MFH is carried out on the short fibre reinforced matrix material to obtain the pseudo-grains elasticity tensors $\mathbb{C}_i(\alpha_i)$, $i = 1, ..., N_\mathrm{s}$, Eq. (1), with $V_\mathrm{I} = V_\mathrm{I}^\mathrm{yarn}$;
- Secondly, using Voigt's rule of mixtures on the aggregate of pure matrix, i.e. the part out of the yarns, and on the short fibre reinforced matrix pseudo-grains, the final homogenised elasticity tensor of a woven unit cell reads,

$$\mathbb{C}^\mathrm{VM} = v_0 \mathbb{C}_0 + \sum_{i=1}^{N_\mathrm{s}} v_i \mathbb{R}^\mathrm{T}(\boldsymbol{\theta}_i) : \mathbb{C}_i(\alpha_i) : \mathbb{R}(\boldsymbol{\theta}_i)\,, \tag{15}$$

  where v_0 is the volume fraction of matrix (outside of the yarns) in a woven unit cell and satisfies $\sum_{i=1}^{N_\mathrm{s}} v_i = 1.0 - v_0$.

Since the matrix volume fraction v_0 is known for a given woven unit cell, the unknown topology parameters involved in this modelling process are the short fibre aspect ratios, α_i with $i = 1, .., N_\mathrm{s}$, the volume fractions, v_i with $\sum_{i=1}^{N_\mathrm{s}} v_i = 1.0 - v_0$, and the orientation angles, $\boldsymbol{\theta}_i$, of the pseudo-grains. Therefore, the homogenised elasticity tensor obtained by the "V-M" model is expressed as $\mathbb{C}^\mathrm{VM}(\boldsymbol{\chi}^\mathrm{VM}|\mathbb{C}_0, \mathbb{C}_\mathrm{I}, V_\mathrm{I})$, where

$$\boldsymbol{\chi}^\mathrm{VM} = \left\{ v_i,\, \boldsymbol{\theta}_i,\, \alpha_i \mid i = 1, ..., N_\mathrm{s};\, \sum_{i=1}^{N_\mathrm{s}} v_i = 1.0 - v_0 \right\}. \tag{16}$$

3.2. Laminate-Voigt-MFH ("LVM") scheme

The "LVM" scheme is illustrated in Fig. 1(c). Compared to the "V-M" model, instead of using the pure matrix part as a pseudo-grain in Voigt's mixture rule, the "LVM" model treats the pure matrix as a ply. The homogenised woven

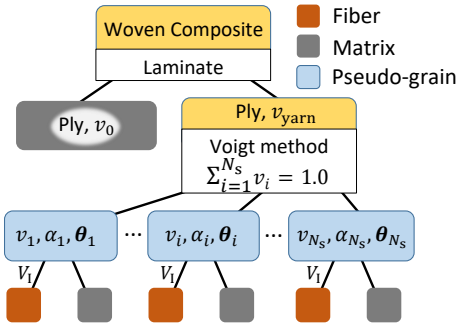

Figure 3: Computational network of the "LVM" scheme.

unit cell is thus modelled by a laminate of pure matrix and Voigt's mixtures of short fibre reinforced matrix pseudo-grains. The detailed bottom to top path of the material network is presented in Fig. 3.

- Firstly, The N_{s} short fibre reinforced matrix pseudo-grains are modelled by MFH to obtain $\mathbb{C}_i(\alpha_i)$, $i = 1, ..., N_{\text{s}}$, Eq. (1), with $V_{\text{I}} = V_{\text{I}}^{\text{yarn}}$;
- Secondly, Voigt's rule of mixture is applied on the aggregate of pseudo short fibre reinforced matrix grains, yielding the elasticity tensor

$$\mathbb{C}_{\text{A}} = \sum_{i=1}^{N_{\text{s}}} v_i \mathbb{R}^{\text{T}}(\boldsymbol{\theta}_i) : \mathbb{C}_i(\alpha_i) : \mathbb{R}(\boldsymbol{\theta}_i)\,, \tag{17}$$

  where the pseudo-grain volume fractions satisfy $\sum_{i=1}^{N_{\text{s}}} v_i = 1.0$.

- Finally, the ply of the pseudo-grains aggregate with a elasticity tensor $\mathbb{C}_{\text{A}}$ is laminated with a pure matrix ply using Eq. (14). This former ply volume volume fraction reads $v_{\text{A}} = 1.0 - v_0$, where v_0 is the volume fraction of matrix, i.e. the out of the yarns phase, in a woven unit cell, and this matrix ply elasticity tensor reads $\mathbb{C}_{\text{B}} = \mathbb{C}_0$.

It appears that the unknown topology parameters involved in the "LVM" scheme are also the short fibre aspect ratios, α_i with $i = 1, .., N_{\text{s}}$, the volume fractions, v_i with $\sum_{i=1}^{N_{\text{s}}} v_i = 1.0$, and the orientation angles, $\boldsymbol{\theta}_i$, of the pseudo-grains. However, the short fibre aspect ratios α_i, and the orientation angles, $\boldsymbol{\theta}_i$, do not have the same values for the "V-M" and "LVM" models. Besides, in the "LVM" model, the volume fractions v_i satisfy $\sum_{i=1}^{N_{\text{s}}} v_i = 1.0$. Finally, we denote the homogenised elasticity tensor obtained by the "LVM" model as $\mathbb{C}^{\text{LVM}}(\boldsymbol{\chi}^{\text{LVM}}|\mathbb{C}_0, \mathbb{C}_{\text{I}}, V_{\text{I}})$, where

$$\boldsymbol{\chi}^{\text{LVM}} = \left\{ v_i,\, \boldsymbol{\theta}_i,\, \alpha_i \mid i = 1, ..., N_{\text{s}};\, \sum_{i=1}^{N_{\text{s}}} v_i = 1.0 \right\}, \tag{18}$$

are the parameters.

3.3. Voigt-Laminate-MFH ("VLM") scheme

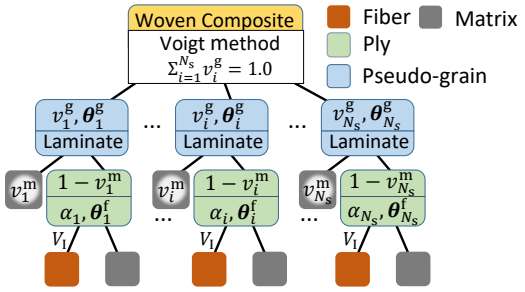

Figure 4: Computational network of the "VLM" scheme.

In the "VLM" model, as illustrated in Fig. 1(d), each pseudo-grain used in Voigt's mixture law is made of a two-ply laminate made of a pure matrix ply and a short fibre reinforced matrix ply. The modelling process of the "VLM" scheme follows the bottom to top path of the material network presented in Fig. 4. The 3-step homogenisation process is as follows.

- Firstly, the short fibre reinforced matrix material plies are modelled using MFH to obtain the elasticity tensors $\mathbb{C}_i(\alpha_i)$, $i = 1, ..., N_\mathrm{s}$, using Eq. (1) with $V_\mathrm{I} = V_\mathrm{I}^\mathrm{yarn}$;

- Secondly, each short fibre reinforced matrix material ply is laminated with a pure matrix ply, i.e. representing the out-of-yarn matrix, using Eq. (14), with the two elasticity tensors $\mathbb{C}_\mathrm{B} = \mathbb{C}_0$ and

$$\mathbb{C}_{\mathrm{A}i} \quad = \quad \mathbb{R}^\mathrm{T}(\boldsymbol{\theta}_i^\mathrm{f}) : \mathbb{C}_i(\alpha_i) : \mathbb{R}(\boldsymbol{\theta}_i^\mathrm{f})\,, \tag{19}$$

  and the volume fraction

$$v_{\mathrm{A}i} \quad = \quad 1.0 - v_i^\mathrm{m}, \qquad i = 1, ..., N_\mathrm{s}\,, \tag{20}$$

  where $\boldsymbol{\theta}_i^\mathrm{f}$ is the orientation angles vector of the short fibres reinforced matrix parts, and v_i^m is the volume fraction of the pure matrix ply in the "i^th" laminate. This yields the pseudo-grains elasticity tensors

$$\mathbb{C}_{\mathrm{L}i} = v_{\mathrm{A}i}[\mathbb{C}_{\mathrm{A}i} - \mathbb{C}_0] : \mathbb{P}_{\mathrm{A}i} + \mathbb{C}_0\,. \tag{21}$$

- Thirdly, the Voigt's rule of mixture is applied on the aggregate of pseudo-grains which are made of a laminate of short fibre reinforced matrix and pure matrix materials. The homogenised elasticity tensor of the woven unit cell thus reads

$$\mathbb{C}^\mathrm{VLM} = \sum_{i=1}^{N_\mathrm{s}} v_i^\mathrm{g} \mathbb{R}^\mathrm{T}(\boldsymbol{\theta}_i^\mathrm{g}) \mathbb{C}_{\mathrm{L}i} \mathbb{R}(\boldsymbol{\theta}_i^\mathrm{g})\,, \tag{22}$$

where $\boldsymbol{\theta}_i^{\mathrm{g}}$ is the orientation angles vector of a laminate, the pseudo-grain volume fractions satisfy $\sum_{i=1}^{N_{\mathrm{s}}} v_i^{\mathrm{g}} = 1$, and $\sum_{i=1}^{N_{\mathrm{s}}} v_i^{\mathrm{g}} v_i^{\mathrm{m}} = v_0$, where v_0 is the volume fraction of matrix in a woven unit cell. It needs to be noted that $v_i^{\mathrm{m}} = 1.0$ is permitted for a pure matrix grain in the model.

The homogenised elasticity tensor of the woven unit cell is denoted as $\mathbb{C}^{\mathrm{VLM}}(\boldsymbol{\chi}^{\mathrm{VLM}}|\mathbb{C}_0, \mathbb{C}_{\mathrm{I}}, V_{\mathrm{I}})$ for the "VLM" model, and the involved topology parameters read

$$\boldsymbol{\chi}^{\mathrm{VLM}} = \left\{ v_i^{\mathrm{g}},\, \boldsymbol{\theta}_i^{\mathrm{g}},\, v_i^{\mathrm{m}},\, \boldsymbol{\theta}_i^{\mathrm{f}},\, \alpha_i \mid i = 1, ..., N_{\mathrm{s}};\, \sum_{i=1}^{N_{\mathrm{s}}} v_i^{\mathrm{g}} = 1.0;\, \sum_{i=1}^{N_{\mathrm{s}}} v_i^{\mathrm{g}} v_i^{\mathrm{m}} = v_0 \right\}. \tag{23}$$

Compared to the "VM" model, besides the short fibre aspect ratios, α_i, the fibre orientation angles, $\boldsymbol{\theta}_i^{\mathrm{f}}$, and the volume fractions of the pseudo-grains in Voigt's mixtures, v_i^{g}, the "VLM" model has extra parameters, such as the rotation angles of the laminates, $\boldsymbol{\theta}_i^{\mathrm{g}}$, and the volume fractions of the matrix in the laminates, v_i^{m}.

4. Learning of the meso-scale material structure parameters $\boldsymbol{\chi}$

Direct Numerical Simulations (DNS) are carried out on woven unit cells in order to generate the so-called training data which correspond to realisations of the homogenised elasticity tensors. The material network parameters $\boldsymbol{\chi}$ (e.g. $\boldsymbol{\chi}^{\mathrm{VM}}$, $\boldsymbol{\chi}^{\mathrm{LVM}}$ and $\boldsymbol{\chi}^{\mathrm{VLM}}$) are thus determined through a learning process using these homogenised elastic properties of the meso-scale material unit cell.

4.1. Training data

The training data are collected from direct computational homogenisation on material unit cells, Fig. 1(a), under the same boundary conditions as considered in the on-line simulations, as it will be discussed in Section 6.2. Since it is not computationally affordable to carry out direct numerical analyses on woven unit with a discretization of the micro-scale details within the yarns, each yarn is treated as a UD fibre reinforced matrix and its mechanical response is computed using the MFH approach with the orientation of the fibres varying with the central axis of the yarn. Such a treatment has been used in [11] and details on the approach are reported in [34] in which predictions are compared to an experimental woven composite system and found to be in good agreement.

The isotropic matrix material is defined by its Young's modulus E_0 and Poisson's ratio ν_0. The transverse isotropic fibres are uniquely defined by five material parameters, two Young's moduli $E_{\mathrm{I}}^{\mathrm{T}}$ and $E_{\mathrm{I}}^{\mathrm{L}}$, respectively for the transverse and longitudinal directions, the major and transverse Poisson's ratios $\nu_{\mathrm{I}}^{\mathrm{LT}}$ and $\nu_{\mathrm{I}}^{\mathrm{TT}}$ and the shear modulus $G_{\mathrm{I}}^{\mathrm{LT}}$. In order to be able to separate the effects of the material micro-structure from that of the material properties in the homogenised results, these parameters are generated repetitively under independent and conditional uniform random distributions. For example, by setting

Table 1: Uniform distribution ranges of material properties with $E_0 = 1.0$.

ν_0	E_I^T	E_I^L	$\nu_\mathrm{I}^\mathrm{LT}$	$\nu_\mathrm{I}^\mathrm{TT}$	G_I^LT
[0.1, 0.45]	[1.5, 30.0]	$[10E_\mathrm{I}^\mathrm{T}, 25E_\mathrm{I}^\mathrm{T}]$	[0.1, 0.45]	[0.1, 0.45]	$[1.0, 1.5E_\mathrm{I}^\mathrm{T}]$

$E_0 = 1.0$, the rest of the parameters are picked randomly from the ranges reported in Tab. 1.

For a given unit cell with a constant fibre volume fraction V_I in the yarns, a series of computational homogenisations is carried out with the generated material properties $\boldsymbol{\gamma} = [E_0, \nu_0, E_\mathrm{I}^\mathrm{T}, E_\mathrm{I}^\mathrm{L}, \nu_\mathrm{I}^\mathrm{LT}, \nu_\mathrm{I}^\mathrm{TT}, G_\mathrm{I}^\mathrm{LT}, V_\mathrm{I}]$. The homogenised elasticity tensor is then denoted by $\hat{\mathbb{C}}(\boldsymbol{\gamma})$.

4.2. Loss function

The loss function is defined as

$$L(\hat{\mathbb{C}},\, \mathbb{C}(\boldsymbol{\chi})) = \frac{1}{n}\sum_{s=1}^{n} \frac{\|\hat{\mathbb{C}}(\boldsymbol{\gamma}_s) - \mathbb{C}(\boldsymbol{\chi}|\boldsymbol{\gamma}_s)\|}{\|\hat{\mathbb{C}}(\boldsymbol{\gamma}_s)\|} + \frac{\lambda}{2} G(\boldsymbol{\chi})\,, \tag{24}$$

where $\|\bullet\|$ refers to the Frobenius norm, n is the number of data used during the training stage, and $\mathbb{C}(\boldsymbol{\chi}|\boldsymbol{\gamma}_s) = \mathbb{C}^\mathrm{VM}(\boldsymbol{\chi}^\mathrm{VM}|\boldsymbol{\gamma}_s)$, $\mathbb{C}^\mathrm{LVM}(\boldsymbol{\chi}^\mathrm{LVM}|\boldsymbol{\gamma}_s)$ or $\mathbb{C}^\mathrm{VLM}(\boldsymbol{\chi}^\mathrm{VLM}|\boldsymbol{\gamma}_s)$ respectively for the three proposed models. The Lagrange multiplier λ is used to enforced the volume fraction consistency expression $G(\boldsymbol{\chi})$, which reads, see Figs. 2, 3 and 4,

$$G(\boldsymbol{\chi}^\mathrm{VM}) = \left(\sum_{i=0}^{N_\mathrm{s}} v_i - 1.0\right)^2 \quad \text{for the "V-M" model}\,; \tag{25}$$

$$G(\boldsymbol{\chi}^\mathrm{LVM}) = \left(\sum_{i=1}^{N_\mathrm{s}} v_i - 1.0\right)^2 \quad \text{for the "LVM" model}\,;\ \text{and} \tag{26}$$

$$G(\boldsymbol{\chi}^\mathrm{VLM}) = \left(\sum_{i=1}^{N_\mathrm{s}} v_i^\mathrm{g} - 1.0\right)^2 + \left(\sum_{i=1}^{N_\mathrm{s}} v_i^\mathrm{g} v_i^\mathrm{m} - v_0\right)^2 + \sum_{i=1}^{N_\mathrm{s}} \mathrm{ReLU}(v_i^\mathrm{m} - 1.0)\,, \tag{27}$$

for the "VLM" model, where the ReLU(*) term, $\mathrm{ReLU}(v_i^\mathrm{m} - 1.0)$, ensures $v_i^\mathrm{m} \leq 1.0$. The learning or training stage is defined as the optimisation process

$$\underline{\boldsymbol{\chi}} = \arg\min_{\boldsymbol{\chi}} L(\hat{\mathbb{C}},\, \mathbb{C}(\boldsymbol{\chi})), \tag{28}$$

with $\boldsymbol{\chi}$ defined by Eqs. (16), (18) or (23) respectively for the "V-M", "LVM" or "VLM" model.

4.3. Training process

4.3.1. Initialisation of $\boldsymbol{\chi}$

First of all, the number of pseudo-grains or short fibre reinforced matrix material parts, N_s, is set with an assumed integer. The, the parameters vector $\boldsymbol{\chi}$ has to be initialised with physically meaningful values.

Volume fractions, v_i, v_i^g and v_i^m. According to the applied reduced order model, a positive random value in (0, 1) is used for v_i in the "V-M" and "LVM" models and for v_i^g in the "VLM" model. The generated v_i or v_i^g are normalised in order to satisfy the constraint of volume fraction consistency. For the "VLM" model, $v_i^\mathrm{m} = v_0$ can be used as initial value.

Orientation angles, $\boldsymbol{\theta}_i$, $\boldsymbol{\theta}_i^g$ and $\boldsymbol{\theta}_i^f$. Orientation angles are in an infinitive range, and can practically be initialised with random values in the range $[-90°, 90°]$. According to the application, reduced angle ranges can be adopted to speed-up the training process.

Short fibre aspect ratios, α_i. High aspect ratio of short fibre is avoided at initialisation, since the homogenised properties are not sensitive to inclusion's aspect ratio of high value, which could bring difficulties in training. Therefore, random values in [10, 100] are used to initialise the different α_i.

4.3.2. Optimisation iterations

A Stochastic Gradient Descent (SGD) algorithm with Adaptive Moment Estimation (Adam) [35] is adopted for the parameters update. In this algorithm, running averages of both the gradients $\nabla L(\boldsymbol{\chi}_t)$ and the second moments of the gradients $(\nabla L(\boldsymbol{\chi}_t))^2$ are used, and the updated parameters vector $\boldsymbol{\chi}_{t+1}$ is given by

$$\begin{aligned}
\boldsymbol{m}_{t+1} &= \kappa_1 \boldsymbol{m}_t + (1-\kappa_1)\nabla L(\boldsymbol{\chi}_t) \\
\boldsymbol{r}_{t+1} &= \kappa_2 \boldsymbol{r}_t + (1-\kappa_2)(\nabla L(\boldsymbol{\chi}_t))^2 \\
\hat{\boldsymbol{m}}_{t+1} &= \frac{\boldsymbol{m}_{t+1}}{1-\kappa_1^{t+1}} \quad \text{and} \quad \hat{\boldsymbol{r}}_{t+1} = \frac{\boldsymbol{r}_{t+1}}{1-\kappa_2^{t+1}} \\
\boldsymbol{\chi}_{t+1} &= \boldsymbol{\chi}_t - \boldsymbol{\eta} \odot \frac{\hat{\boldsymbol{m}}_{t+1}}{\sqrt{\hat{\boldsymbol{r}}_{t+1}} + \epsilon}\,,
\end{aligned} \tag{29}$$

where t is the iteration step, ϵ is a small scale, e.g. 10^{-8}, used to avoid division by 0, $\boldsymbol{\eta}$ is the learning rate, κ_1 and κ_2 are the two forgetting factors related to the gradients and second moments of gradients, respectively, and taken as $\kappa_1 = 0.9$ and $\kappa_2 = 0.999$. Because the volume fraction v_i (v_i^g and v_i^m), orientation angles $\boldsymbol{\theta}_i$ ($\boldsymbol{\theta}_i^\mathrm{g}$ and $\boldsymbol{\theta}_i^\mathrm{f}$) and short fibre aspect ratios α_i, all have different units and data ranges, different learning rates respectively η_v, η_α and η_θ are used, e.g. for the "V-M" and "LVM" models $\boldsymbol{\eta}^\mathrm{VM} = \boldsymbol{\eta}^\mathrm{LVM} = \{\eta_v, \eta_\theta, \eta_\alpha\}$, and for the "VLM" model $\boldsymbol{\eta}^\mathrm{VLM} = \{\eta_v, \eta_{\theta\mathrm{g}}, \eta_{v\mathrm{m}}, \eta_{\theta\mathrm{f}}, \eta_\alpha\}$. In the set of relations (29), the $(\bullet)^2$, $\sqrt{\bullet}$ and $\odot$ operators are meant to be the element-wise square, square-root and

product operators. The gradient $\nabla L(\boldsymbol{\chi})$ can be computed efficiently using the chain rule of partial derivatives, with more details provided in Appendix B.

In order to avoid negative volume fractions, a ReLU function is used to modify the update of the volume fraction v_i (v_i^{g} and v_i^{m}), i.e.

$$v_{it+1} = \mathrm{ReLU}(v_{it} + \Delta v_{it+1}) \,, \quad i = 0, 1, .., N_{\mathrm{s}} \,. \tag{30}$$

Finally, when a pseudo-grain reaches $v_i = 0.0$ ($v_i^{\mathrm{g}} = 0.0$), this grain is deactivated in the system, and will not be reactivated. Therefore, the final number of pseudo-grains $\underline{N}_{\mathrm{s}}$ will be equal or lower than the starting number N_{s}, $\underline{N}_{\mathrm{s}} \leq N_{\mathrm{s}}$. A proper learning rate η_v is essential to balance the speed of pseudo-grain deactivation and the speed of parameters training.

The dimension of the resulting $\underline{\boldsymbol{\chi}}$ could be reduced by merging the pseudo-grains, i, $j = 1, ..., \underline{N}_{\mathrm{s}}$, $i \neq j$,

- if $\boldsymbol{\theta}_i \approx \boldsymbol{\theta}_j$ and $\alpha_i \approx \alpha_j$, in $\underline{\boldsymbol{\chi}}^{\mathrm{VM}}$ and $\underline{\boldsymbol{\chi}}^{\mathrm{LVM}}$;
- if $\boldsymbol{\theta}_i^{\mathrm{g}} \approx \boldsymbol{\theta}_j^{\mathrm{g}}$, $v_i^{\mathrm{m}} \approx v_j^{\mathrm{m}}$, $\boldsymbol{\theta}_i^{\mathrm{f}} \approx \boldsymbol{\theta}_j^{\mathrm{f}}$ and $\alpha_i \approx \alpha_j$ in $\underline{\boldsymbol{\chi}}^{\mathrm{VLM}}$.

5. Nonlinear analyses using the meso-scale material networks on-line

The proposed meso-scale material models are presented in forms of networks, see Figs. 2, 3 and 4, which give the information paths and the related computation operations. The material networks are completely determined by their corresponding set of parameters $\underline{\boldsymbol{\chi}}$ that can be obtained through the learning stage presented in Section 4. Once these parameters determined, nonlinear analyses can be carried out through the material networks.

Following the information paths of a material network, the strain increment of a material node is first distributed from top to bottom to its descendant nodes at each network level, until reaching the matrix and fibre phases at the bottom of the network. Then, the stresses and internal variables of these material nodes are submitted to their parent nodes. According to the material model type of the parent nodes, different strain increment distribution rules are used, and some nonlinear equations need to be solved using the stresses and internal variables submitted by their descendant nodes. Iterations are normally needed between parent and descendant nodes, until the required nonlinear equation at the highest material node is balanced.

In general, for all the involved composite material nodes, the distribution of a strain increment satisfies

$$\Delta\boldsymbol{\varepsilon} = \sum_{n=1}^{N_{\mathrm{d}}} v_n^{\mathrm{d}} \Delta\boldsymbol{\varepsilon}_n^{\mathrm{d}} \,, \tag{31}$$

where $\Delta\boldsymbol{\varepsilon}$ is the strain increment of a parent node which has N_{d} direct descendant nodes, the strain increments of these nodes are $\Delta\boldsymbol{\varepsilon}_n^{\mathrm{d}}$, $n = 1, ..., N_{\mathrm{d}}$, and their volume fractions satisfy $\sum_{n=1}^{N_{\mathrm{d}}} v_n^{\mathrm{d}} = 1.0$. Similarly, the stress of the

parent node, $\boldsymbol{\sigma}$, is computed from the stresses, $\boldsymbol{\sigma}_n^{\mathrm{d}}$, submitted from its direct descendant nodes following,

$$\boldsymbol{\sigma} = \sum_{n=1}^{N_{\mathrm{d}}} v_n^{\mathrm{d}} \boldsymbol{\sigma}_n^{\mathrm{d}} \,. \tag{32}$$

Therefore, the algorithmic operator can be deduced directly by

$$\mathbb{C}^{\mathrm{alg}} = \frac{\mathrm{d}\boldsymbol{\sigma}}{\mathrm{d}\boldsymbol{\varepsilon}} \quad = \quad \sum_{n=1}^{N_{\mathrm{d}}} v_n^{\mathrm{d}} \frac{\mathrm{d}\boldsymbol{\sigma}_n^{\mathrm{d}}}{\mathrm{d}\boldsymbol{\varepsilon}_n^{\mathrm{d}}} : \frac{\mathrm{d}\boldsymbol{\varepsilon}_n^{\mathrm{d}}}{\mathrm{d}\boldsymbol{\varepsilon}} = \sum_{n=1}^{N_{\mathrm{d}}} v_n^{\mathrm{d}} \mathbb{C}_n^{\mathrm{alg,\ d}} : \frac{\mathrm{d}\boldsymbol{\varepsilon}_n^{\mathrm{d}}}{\mathrm{d}\boldsymbol{\varepsilon}} \,, \tag{33}$$

where $\mathbb{C}_n^{\mathrm{alg,\ d}}$ is the algorithmic operator of a direct descendant material node, and the terms $\frac{\mathrm{d}\boldsymbol{\varepsilon}_n^{\mathrm{d}}}{\mathrm{d}\boldsymbol{\varepsilon}}$ are resolved through the strain distribution rule and nonlinear equations of the parent material model.

The strain distribution rule and nonlinear equations of the parent material node models are now briefly recalled. All the expressions are expressed in the principal coordinates of the parent material node to avoid redundant rotation operations.

5.1. Node using MFH to homogenise the short fibre reinforced matrix

For a parent node corresponding to the MFH model and whose descendant nodes experience elasto-plastic/elasto-visco-plastic deformations, the homogenised response is solved in an incremental form through a so-called Linear Comparison Composite (LCC) [36, 37]. The LCC is a virtual linear heterogeneous material whose constituents behaviours are defined by virtual elastic operators matching the linearised behaviours of the real composite material constituents at a given strain state. Among the different linearisation techniques developed in order to define the LCC, the incremental-secant approach [38, 39] is considered in this work, because of its accuracy for non-proportional loading and strain softening cases [40].

Since the nodes solved by MFH involve a 2-phase composite material, in this section, we use the subscripts "I" and "0" to refer to respectively the short fibre inclusion phase ω_{I} and the matrix phase ω_0. The absence of subscript refers to the homogenised values.

5.1.1. Incremental secant virtual elastic operator [38, 39]

During a time increment $[t^n,\ t^{n+1}]$, the composite material is first subjected to a virtual elastic unloading from the configuration at time t^n to reach a residual state so that $\boldsymbol{\sigma}^{\mathrm{res},\,n} = 0$, where the superscript "res" refers to the virtually unloaded state. Then, the composite material is loaded to the new configuration at time t^{n+1}, see Fig. 5(a).

Since the virtual unloading is elastic, the residual state of the composite material and of its phases is fully determined by the linear elastic MFH formula presented in Section 2.1. Then, from the residual state, $\boldsymbol{\varepsilon}^{\mathrm{res},\,n}$ and $\boldsymbol{\sigma}^{\mathrm{res},\,n} = 0$,

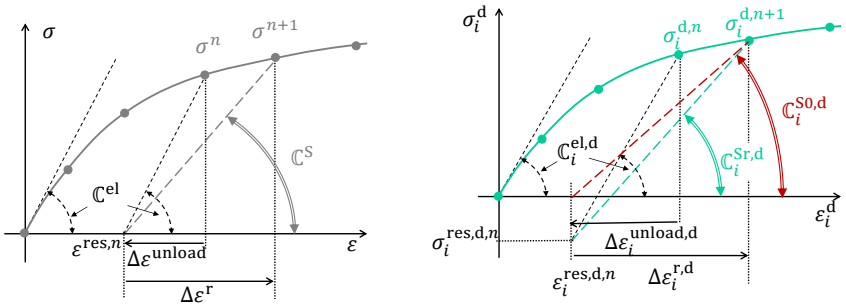

(a) Composite (b) Phase ω_i

Figure 5: Definition of the LCC in the incremental-secant method for elasto-plastic composites.

at t^n, the secant linearisation of the non-linear composite material is carried out with the strain increment $\Delta\boldsymbol{\varepsilon}^{\mathrm{r}}$ defined such that

$$\boldsymbol{\varepsilon}^{n+1} = \boldsymbol{\varepsilon}^{\mathrm{res},\,n} + \Delta\boldsymbol{\varepsilon}^{\mathrm{r}}\,, \tag{34}$$

where $\boldsymbol{\varepsilon}^{n+1}$ is a known value at the homogenised level. Similarly, the phases strain increments $\Delta\boldsymbol{\varepsilon}_i^{\mathrm{r},\,\mathrm{d}}$ are defined such that

$$\boldsymbol{\varepsilon}_i^{\mathrm{d},\,n+1} = \boldsymbol{\varepsilon}_i^{\mathrm{res},\,\mathrm{d},\,n} + \Delta\boldsymbol{\varepsilon}_i^{\mathrm{r},\,\mathrm{d}}\,, \tag{35}$$

as illustrated in Fig. 5(b), where $i =$ "0" or "I" respectively refers to the matrix or inclusion phase. Finally, in each phase, an incremental-secant operator $\mathbb{C}_i^{\mathrm{S,d}} = \mathbb{C}_i^{\mathrm{Sr},\,\mathrm{d}}$ or $\mathbb{C}_i^{\mathrm{S,d}} = \mathbb{C}_i^{\mathrm{S0},\,\mathrm{d}}$ is defined from the phase residual stress-strain state (which does not necessarily vanish). The former expression evaluates the incremental-secant operator from the stress residual, but has been shown to result in too stiff results when used in the matrix phase of a stiff inclusion composite material. The latter expression computes the incremental-secant operator from a zero-stress state and is used in the matrix phase. These incremental-secant operators are defined such that

$$\boldsymbol{\sigma}_i^{\mathrm{d},\,n+1} = \boldsymbol{\sigma}_i^{\mathrm{res},\,\mathrm{d},\,n} + \mathbb{C}_i^{\mathrm{Sr,d}} : \Delta\boldsymbol{\varepsilon}_i^{\mathrm{r},\,\mathrm{d}} \text{ or } \boldsymbol{\sigma}_i^{\mathrm{d},\,n+1} = \mathbb{C}_i^{\mathrm{S0},\,\mathrm{d}} : \Delta\boldsymbol{\varepsilon}_i^{\mathrm{r},\,\mathrm{d}}\,. \tag{36}$$

Therefore, the LCC is defined using the incremental-secant operators $\mathbb{C}_i^{\mathrm{S},\,\mathrm{d}}$, and the set of Eqs. (1-2) is thus rewritten using $\mathbb{C}_0^{\mathrm{S},\,\mathrm{d}}$ and $\mathbb{C}_{\mathrm{I}}^{\mathrm{S},\,\mathrm{d}}$ as operators $\mathbb{C}_0$ and $\mathbb{C}_{\mathrm{I}}$.

Finally, the homogenised stress in the incremental-secant formalism reads

$$\boldsymbol{\sigma} = \Delta\boldsymbol{\sigma}^{\mathrm{r}} = \mathbb{C}^{\mathrm{S}}(\mathrm{I}, \mathbb{C}_0^{\mathrm{S},\,\mathrm{d}}, \mathbb{C}_{\mathrm{I}}^{\mathrm{S},\,\mathrm{d}}, V_{\mathrm{I}}) : \Delta\boldsymbol{\varepsilon}^{\mathrm{r}}\,, \text{ with} \tag{37}$$

$$\mathbb{C}^{\mathrm{S}} = \left[V_{\mathrm{I}}\mathbb{C}_{\mathrm{I}}^{\mathrm{S},\,\mathrm{d}} : \mathbb{B}^{\epsilon}(\mathrm{I}, \mathbb{C}_0^{\mathrm{S},\,\mathrm{d}}, \mathbb{C}_{\mathrm{I}}^{\mathrm{S},\,\mathrm{d}}) + V_0\mathbb{C}_0^{\mathrm{S},\,\mathrm{d}}\right] : \left[V_{\mathrm{I}}\mathbb{B}^{\epsilon}(\mathrm{I}, \mathbb{C}_0^{\mathrm{S},\,\mathrm{d}}, \mathbb{C}_{\mathrm{I}}^{\mathrm{S},\,\mathrm{d}}) + V_0\mathbb{I}\right]^{-1}\,, \tag{38}$$

where $V_0 = 1 - V_{\mathrm{I}}$ is the matrix volume fraction in the yarns, and where the superscript "$n+1$" is omitted without introducing any ambiguity.

5.1.2. Nonlinear equations resolution

The resolution of the MFH equations (37-38) is equivalent to the resolution of a nonlinear system of equations stated as $\mathcal{F}^{\mathrm{M}} = \mathbf{0}$, where $\mathcal{F}^{\mathrm{M}}$ is the inclusion phase stress residual vector. For a time step $[t^n, t^{n+1}]$, where $\Delta\boldsymbol{\varepsilon}^{\mathrm{r}}$ is known, this inclusion phase stress residual vector reads, see [41, e.g],

$$\begin{aligned}\mathcal{F}^{\mathrm{M}} &= \mathbb{C}_0^{\mathrm{S},\,\mathrm{d}} : \\ &\quad [\Delta\boldsymbol{\varepsilon}_{\mathrm{I}}^{\mathrm{r},\,\mathrm{d}} - \frac{1}{V_0}\left(\mathbb{S}(\mathrm{I}, \mathbb{C}_0^{\mathrm{S},\,\mathrm{d}})\right)^{-1} : (\Delta\boldsymbol{\varepsilon}_{\mathrm{I}}^{\mathrm{r},\,\mathrm{d}} - \Delta\boldsymbol{\varepsilon}^{\mathrm{r}})] - \mathbb{C}_{\mathrm{I}}^{\mathrm{S},\,\mathrm{d}} : \Delta\boldsymbol{\varepsilon}_{\mathrm{I}}^{\mathrm{r},\,\mathrm{d}} \end{aligned} \quad (39)$$

An iterative process is carried out on the strain increment $\Delta\boldsymbol{\varepsilon}_{\mathrm{I}}^{\mathrm{r},\,\mathrm{d}}$, until the residual vector satisfies the condition $|\mathcal{F}^{\mathrm{M}}| \leq \mathrm{Tol}$. We define the Jacobian, which reads

$$\begin{aligned}\mathcal{J}_{\mathrm{I}} &= \frac{\mathrm{d}\mathcal{F}^{\mathrm{M}}}{\mathrm{d}\boldsymbol{\varepsilon}_{\mathrm{I}}^{\mathrm{d}}} = \frac{\partial\mathcal{F}^{\mathrm{M}}}{\partial\boldsymbol{\varepsilon}_{\mathrm{I}}^{\mathrm{d}}} + \frac{\partial\mathcal{F}^{\mathrm{M}}}{\partial\boldsymbol{\varepsilon}_0^{\mathrm{d}}} : \frac{\partial\boldsymbol{\varepsilon}_0^{\mathrm{d}}}{\partial\boldsymbol{\varepsilon}_{\mathrm{I}}^{\mathrm{d}}} \\ &= \mathbb{C}_0^{\mathrm{S},\,\mathrm{d}} : \left[\mathbb{I} - \mathbb{S}^{-1}\right] - \mathbb{C}_{\mathrm{I}}^{\mathrm{S},\,\mathrm{d}} - \frac{\partial\mathbb{C}_{\mathrm{I}}^{\mathrm{S},\,\mathrm{d}}}{\partial\boldsymbol{\varepsilon}_{\mathrm{I}}^{\mathrm{d}}} : \Delta\boldsymbol{\varepsilon}_{\mathrm{I}}^{\mathrm{r},\,\mathrm{d}} - \\ &\quad \frac{V_{\mathrm{I}}}{V_0}\frac{\partial\mathbb{C}_0^{\mathrm{S},\,\mathrm{d}}}{\partial\boldsymbol{\varepsilon}_0^{\mathrm{d}}} : \left[\Delta\boldsymbol{\varepsilon}_{\mathrm{I}}^{\mathrm{r},\,\mathrm{d}} - \mathbb{S}^{-1} : \frac{\left(\Delta\boldsymbol{\varepsilon}_{\mathrm{I}}^{\mathrm{r},\,\mathrm{d}} - \Delta\boldsymbol{\varepsilon}^{\mathrm{r}}\right)}{v_0}\right] - \\ &\quad \frac{V_{\mathrm{I}}}{V_0^2}\mathbb{C}_0^{\mathrm{S},\,\mathrm{d}} \otimes (\Delta\boldsymbol{\varepsilon}_{\mathrm{I}}^{\mathrm{r},\,\mathrm{d}} - \Delta\boldsymbol{\varepsilon}^{\mathrm{r}}) :: (\mathbb{S}^{-1} \otimes \mathbb{S}^{-1}) :: \frac{\partial\mathbb{S}}{\partial\boldsymbol{\varepsilon}_0^{\mathrm{d}}} - \\ &\quad \frac{V_{\mathrm{I}}}{V_0}\mathbb{C}_0^{\mathrm{S},\,\mathrm{d}} : \mathbb{S}^{-1}\,, \end{aligned} \quad (40)$$

so that the strain increment correction in the inclusion phase reads

$$\Delta\boldsymbol{\varepsilon}_{\mathrm{I}}^{\mathrm{r},\,\mathrm{d}} \leftarrow \Delta\boldsymbol{\varepsilon}_{\mathrm{I}}^{\mathrm{r},\,\mathrm{d}} + \boldsymbol{c}_{\boldsymbol{\varepsilon}_{\mathrm{I}}} \;\text{ with } \boldsymbol{c}_{\boldsymbol{\varepsilon}_{\mathrm{I}}} = -\mathcal{J}_{\mathrm{I}}^{-1} : \mathcal{F}^{\mathrm{M}}\,. \quad (41)$$

After convergence, we can evaluate

$$\frac{\mathrm{d}\boldsymbol{\varepsilon}_{\mathrm{I}}^{\mathrm{d}}}{\mathrm{d}\boldsymbol{\varepsilon}} = -\mathcal{J}_{\mathrm{I}}^{-1} : \frac{\partial\mathcal{F}^{\mathrm{M}}}{\partial\boldsymbol{\varepsilon}}\,, \text{ and } \quad \frac{\mathrm{d}\boldsymbol{\varepsilon}_0^{\mathrm{d}}}{\mathrm{d}\boldsymbol{\varepsilon}} = \frac{1}{V_0}(\mathbb{I} - V_{\mathrm{I}}\frac{\mathrm{d}\boldsymbol{\varepsilon}_{\mathrm{I}}^{\mathrm{d}}}{\mathrm{d}\boldsymbol{\varepsilon}})\,. \quad (42)$$

The homogenised stress $\boldsymbol{\sigma}$ and algorithmic operator $\mathbb{C}^{\mathrm{alg}}$ can be deduced using Eqs. (32) and (33), which yield

$$\boldsymbol{\sigma} = V_{\mathrm{I}}\boldsymbol{\sigma}_{\mathrm{I}}^{\mathrm{d}} + V_0\boldsymbol{\sigma}_0^{\mathrm{d}}\,, \quad (43)$$

and

$$\mathbb{C}^{\mathrm{alg}} = V_{\mathrm{I}}\mathbb{C}_{\mathrm{I}}^{\mathrm{alg},\,\mathrm{d}} : \frac{\mathrm{d}\boldsymbol{\varepsilon}_{\mathrm{I}}^{\mathrm{d}}}{\mathrm{d}\boldsymbol{\varepsilon}} + V_0\mathbb{C}_0^{\mathrm{alg},\,\mathrm{d}} : \frac{\mathrm{d}\boldsymbol{\varepsilon}_0^{\mathrm{d}}}{\mathrm{d}\boldsymbol{\varepsilon}}\,, \quad (44)$$

where $\mathbb{C}_{\mathrm{I}}^{\mathrm{alg},\,\mathrm{d}}$ and $\mathbb{C}_0^{\mathrm{alg},\,\mathrm{d}}$ are the algorithmic operators of respectively the fibre and matrix material models.

More details, including the tensors derivatives can be found in [38] and [39] for the first and second statistical moments schemes, respectively.

5.2. Node using Voigt's mixture model to homogenised the pseudo-grains

For a parent material node using Voigt's mixture rule, all its direct descendant nodes have the same strain, i.e. $\Delta\boldsymbol{\varepsilon}_n^{\mathrm{d}} = \Delta\boldsymbol{\varepsilon}$, $n = 1, ..., N_{\mathrm{d}}$. There are no extra nonlinear equations that need to be solved at this parent node and its stress is directly computed by Eq. (32). Since $\frac{\mathrm{d}\boldsymbol{\varepsilon}_n^{\mathrm{d}}}{\mathrm{d}\boldsymbol{\varepsilon}} = \mathbb{I}$, the algorithmic operator of the Voigt's mixture model reads

$$\mathbb{C}^{\mathrm{alg}} = \sum_{n=1}^{N_{\mathrm{d}}} v_n^{\mathrm{d}} \mathbb{C}_n^{\mathrm{alg,\ d}} \,. \tag{45}$$

5.3. Node using the two-ply laminate theory

The nonlinear two-ply laminate problem, with the two phases referred to by the subscripts "A" and "B", can be written as a nonlinear equation, which reads

$$\mathcal{F}^{\mathrm{L}} = \mathbb{M}_{\mathrm{o}} : (\boldsymbol{\sigma}_{\mathrm{A}}^{\mathrm{d}} - \boldsymbol{\sigma}_{\mathrm{B}}^{\mathrm{d}}) + \mathbb{M}_{\mathrm{I}} : (\boldsymbol{\varepsilon}_{\mathrm{A}}^{\mathrm{d}} - \boldsymbol{\varepsilon}) = \mathbf{0} \,, \tag{46}$$

where the two tensor operators $\mathbb{M}_{\mathrm{o}}$ and $\mathbb{M}_{\mathrm{I}}$ were defined in Section 2.3. At each time increment, Eq. (46) is solved through Newton-Raphson iterations, e.g. iterating on the value of $\boldsymbol{\varepsilon}_{\mathrm{A}}^{\mathrm{d}}$ under constant $\boldsymbol{\varepsilon}$. Since

$$\begin{aligned} \delta\mathcal{F}^{\mathrm{L}} &= \mathbb{M}_{\mathrm{o}} : (\delta\boldsymbol{\sigma}_{\mathrm{A}}^{\mathrm{d}} - \delta\boldsymbol{\sigma}_{\mathrm{B}}^{\mathrm{d}}) + \mathbb{M}_{\mathrm{I}} : (\delta\boldsymbol{\varepsilon}_{\mathrm{A}}^{\mathrm{d}} - \delta\boldsymbol{\varepsilon}) \\ &= \mathbb{M}_{\mathrm{o}} : (\mathbb{C}_{\mathrm{A}}^{\mathrm{alg,\ d}} : \delta\boldsymbol{\varepsilon}_{\mathrm{A}}^{\mathrm{d}} - \mathbb{C}_{\mathrm{B}}^{\mathrm{alg,\ d}} : \delta\boldsymbol{\varepsilon}_{\mathrm{B}}^{\mathrm{d}}) + \mathbb{M}_{\mathrm{I}} : (\delta\boldsymbol{\varepsilon}_{\mathrm{A}}^{\mathrm{d}} - \delta\boldsymbol{\varepsilon}) \,, \end{aligned} \tag{47}$$

using Eq. (6) leads to

$$\begin{aligned} \delta\mathcal{F}^{\mathrm{L}} &= \mathbb{M}_{\mathrm{o}} : \left[\mathbb{C}_{\mathrm{A}}^{\mathrm{alg,\ d}} : \delta\boldsymbol{\varepsilon}_{\mathrm{A}}^{\mathrm{d}} - \mathbb{C}_{\mathrm{B}}^{\mathrm{alg,\ d}} : (\frac{1}{v_{\mathrm{B}}^{\mathrm{d}}}\delta\boldsymbol{\varepsilon} - \frac{v_{\mathrm{A}}^{\mathrm{d}}}{v_{\mathrm{B}}^{\mathrm{d}}}\delta\boldsymbol{\varepsilon}_{\mathrm{A}}^{\mathrm{d}})\right] + \mathbb{M}_{\mathrm{I}} : (\delta\boldsymbol{\varepsilon}_{\mathrm{A}}^{\mathrm{d}} - \delta\boldsymbol{\varepsilon}) \\ &= \left[\mathbb{M}_{\mathrm{o}} : (\mathbb{C}_{\mathrm{A}}^{\mathrm{alg,\ d}} + \frac{v_{\mathrm{A}}^{\mathrm{d}}}{v_{\mathrm{B}}^{\mathrm{d}}}\mathbb{C}_{\mathrm{B}}^{\mathrm{alg,\ d}}) + \mathbb{M}_{\mathrm{I}}\right] : \delta\boldsymbol{\varepsilon}_{\mathrm{A}}^{\mathrm{d}} - \left[\frac{1}{v_{\mathrm{B}}^{\mathrm{d}}}\mathbb{M}_{\mathrm{o}} : \mathbb{C}_{\mathrm{B}}^{\mathrm{alg,\ d}} + \mathbb{M}_{\mathrm{I}}\right] : \delta\boldsymbol{\varepsilon} \,. \end{aligned} \tag{48}$$

We define the Jacobian

$$\mathcal{J}_{\mathrm{A}} = \frac{\mathrm{d}\mathcal{F}^{\mathrm{L}}}{\mathrm{d}\boldsymbol{\varepsilon}_{\mathrm{A}}^{\mathrm{d}}} = \left[\mathbb{M}_{\mathrm{o}} : \left(\mathbb{C}_{\mathrm{A}}^{\mathrm{alg,\ d}} + \frac{v_{\mathrm{A}}^{\mathrm{d}}}{v_{\mathrm{B}}^{\mathrm{d}}}\mathbb{C}_{\mathrm{B}}^{\mathrm{alg,\ d}}\right) + \mathbb{M}_{\mathrm{I}}\right] \,, \tag{49}$$

with $\boldsymbol{\varepsilon}$ constant during an incremental step. Therefore the system $\mathcal{F}^{\mathrm{L}} = \mathbf{0}$ is solved by iterating on $\boldsymbol{\varepsilon}_{\mathrm{A}}^{\mathrm{d}}$. After convergence, using

$$\frac{\mathrm{d}\mathcal{F}^{\mathrm{L}}}{\mathrm{d}\boldsymbol{\varepsilon}} = -\left[\frac{1}{v_{\mathrm{B}}^{\mathrm{d}}}\mathbb{M}_{\mathrm{o}} : \mathbb{C}_{\mathrm{B}}^{\mathrm{alg,\ d}} + \mathbb{M}_{\mathrm{I}}\right] \,, \tag{50}$$

we have

$$\frac{\mathrm{d}\boldsymbol{\varepsilon}_{\mathrm{A}}^{\mathrm{d}}}{\mathrm{d}\boldsymbol{\varepsilon}} = -\mathcal{J}_{\mathrm{A}}^{-1} : \frac{\mathrm{d}\mathcal{F}^{\mathrm{L}}}{\mathrm{d}\boldsymbol{\varepsilon}} \quad \text{and} \quad \frac{\mathrm{d}\boldsymbol{\varepsilon}_{\mathrm{B}}^{\mathrm{d}}}{\mathrm{d}\boldsymbol{\varepsilon}} = \frac{1}{v_{\mathrm{B}}^{\mathrm{d}}}(\mathbb{I} - v_{\mathrm{A}}^{\mathrm{d}}\frac{\mathrm{d}\boldsymbol{\varepsilon}_{\mathrm{A}}^{\mathrm{d}}}{\mathrm{d}\boldsymbol{\varepsilon}}) \,. \tag{51}$$

Then the algorithmic operator of the laminate, Eq. (33), reads

$$\mathbb{C}^{\mathrm{alg}} = v_{\mathrm{A}}^{\mathrm{d}}\mathbb{C}_{\mathrm{A}}^{\mathrm{alg,\ d}}\frac{\mathrm{d}\boldsymbol{\varepsilon}_{\mathrm{A}}^{\mathrm{d}}}{\mathrm{d}\boldsymbol{\varepsilon}} + v_{\mathrm{B}}^{\mathrm{d}}\mathbb{C}_{\mathrm{B}}^{\mathrm{alg,\ d}}\frac{\mathrm{d}\boldsymbol{\varepsilon}_{\mathrm{B}}^{\mathrm{d}}}{\mathrm{d}\boldsymbol{\varepsilon}} \,. \tag{52}$$

Table 2: Description of the two unit cells: volume fractions of fibre in a yarn $V_{\mathrm{I}}^{\mathrm{yarn}}$, yarn in a unit cell v_{yarn}, and matrix in a unit cell v_0; and number of elements and number of degrees of freedom for the two meshes.

Unit cell	$V_{\mathrm{I}}^{\mathrm{yarn}}$	v_{yarn}	v_0	Number of elements	Number of degrees of freedom
#1	65%	48.32%	51.68%	85909	42149
#2	85%	64.56%	35.44%	63189	31085

6. Application to woven composites

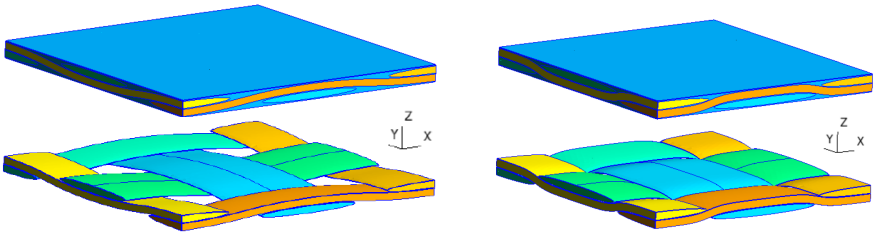

(a) Unit cell #1 (b) Unit cell #2

Figure 6: Two woven unit cells (up) and their yarns (below) with (a) 48.32% and (b) 64.56% of yarn volume fractions.

In this section, the proposed models are applied to predict the non-linear behaviour of the plain woven unit cells and the simulation results are verified with direct numerical simulations. The considered bidirectional fabric reinforced matrix unit cells of type "Plain" 1-1 are illustrated in Fig. 6. Two volume fractions of yarns are successively considered as reported in Tab. 2. The generation process of the micro-structure is detailed in [34].

It can be seen that unit cell "#2" is more compact than unit cell "#1". We note that unit cell "#2" corresponds the geometry of woven composite AS4/8552 [34].

The unit cells are meshed with linear tetrahedra using element-averaged volume deformation in order to alleviate locking for the elasto-plastic simulations. The numbers of elements and of degrees of freedom are reported in Tab. 2. The yarns are treated as UD fibre reinforced matrix whose material response is computed using the MFH approach with the orientation of the fibres varying with the central axis of the yarn as detailed in [34].

6.1. Dimension reduction of $\boldsymbol{\chi}$ according to the geometrical characteristics of the studied woven composites

According to the geometrical characteristics of the studied woven composites, some simplifications can be applied to reduce the number of parameters that

need to be trained, i.e. to reduce the dimension of $\boldsymbol{\chi}$. We use "x-y" for the in-plane directions and "z" for the out-of-plane direction. Besides, the fibre longitudinal direction is oriented along its local "z"- direction. Using Euler angles $(z - x' - z'')$, the orientations of pseudo-grains can be written, see Fig. 6,

- For the "V-M" and "LVM" models, as $\boldsymbol{\theta}_i = [0°,\, \theta_i,\, 0°]$ for warp yarns and as $\boldsymbol{\theta}_i = [90°,\, \theta_i,\, 0°]$ for weft yarns;
- For the "VLM" model, as $\boldsymbol{\theta}_i^{\mathrm{g}} = [0°,\, \theta_i^{\mathrm{g}},\, 0°]$, $\boldsymbol{\theta}_i^{\mathrm{f}} = [0°,\, \theta_i^{\mathrm{f}},\, 0°]$ for warp yarns and $\boldsymbol{\theta}_i^{\mathrm{g}} = [90°,\, \theta_i^{\mathrm{g}},\, 0°]$, $\boldsymbol{\theta}_i^{\mathrm{f}} = [90°,\, \theta_i^{\mathrm{f}},\, 0°]$ for weft yarns.

Besides, this bidirectional fabric reinforced matrix being of type "Plain" 1-1, because of the rotational symmetry in the warp and weft directions, it has identical properties in along these two in-plane orthogonal principal directions. Therefore, in the optimisation Eq. (28), only the parameters of half of the short fibre reinforced matrix pseudo-grains need to be considered, e.g. the parameters related to the warp yarn.

For all of the three proposed models, when Voigt's rule of mixture is applied, the homogenised elasticity tensor can be computed as

$$\mathbb{C}^{\mathrm{VT}} = \frac{1}{2}(\mathbb{C}^{\mathrm{warp}} + \mathbb{P}^{\mathrm{T}} : \mathbb{C}^{\mathrm{warp}} : \mathbb{P})\,, \tag{53}$$

where $\mathbb{C}^{\mathrm{warp}}$ is the Voigt estimate of the elasticity tensor for an aggregate of pseudo gains of constrained fibre orientations, which are related to the warp only, and $\mathbb{P}$ is the rotation tensor corresponding to a 90° in-plane rotation. Therefore, the dimension of $\boldsymbol{\chi}$, the vector of parameters to be determined, is reduced by half.

6.2. Boundary conditions and training stage

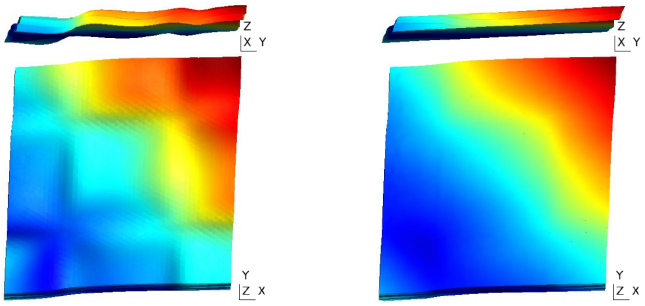

(a) (b)

Figure 7: Effect of boundary conditions on the response of a woven unit cell: deformation of the woven unit cell under (a) full Periodic Boundary Conditions (PBC); (b) Mixed Boundary Conditions (MBC) in which PBC is applied on the surfaces with in-plane normal.

The required training data are realisations of the homogenised elasticity tensor of the woven unit cells which are extracted through direct numerical simulations from the cell simulations with random material parameters, see Section 4. Different boundary conditions can be applied on the unit cells and different homogenised elasticity tensors are yielded. Because of the periodicity of woven composites, periodic boundary condition is a popular choice. However, in a real laminate of woven composites, the material periodicity is seldom satisfied in the out-plane direction. Two kinds of boundary conditions are considered in this work to extract the training data. The first one is a fully Periodic Boundary Condition (PBC) on all the surfaces of the unit cells, and the second one is a Mixed Boundary Condition (MBC) type which keeps periodic boundary conditions on the surfaces with normal along the "x" and "y" in-plane directions, see Fig. 6, and keeps the two surfaces with normal along the "z" out-of-plane direction flat. The effects of the boundary conditions on the deformation of the woven unit cell are presented in Fig. 7 for unit cell "#2" under the same deformation gradient, and in which the deformation is magnified for visualisation purpose.

Using the two different kinds of boundary conditions, we have compared the homogenised in-plane Poisson ratios, ν_{xy}, of unit cell "#2", which corresponds to the geometry of the woven AS4/8552 composite material [34]. The obtained ν_{xy} under PBC (order of 0.1-0.5) is around 10 time higher than that under MBC (order of 0.01-0.1). Experimental measurements of in-plane Poisson ratio on a woven composite yield $\nu_{xy} \in (0.03, 0.05)$ at low strain rate in [42]. However, the analytical result [43] and experimental measurement [44] of the in-plane Poisson ratios for woven fabric have shown $\nu_{xy} \in (0.2, 0.57)$. It indicates that the homogenised elasticity properties of woven composites obtained under MBC are more physical than that obtained under PBC.

6.3. Training results for two woven unit cells

The fibre and yarn volume fractions of the two considered woven unit cells are listed in Tab. 2. The pseudo-grain number related to warp is initialised with $N_\mathrm{s}/2 = 20$. According to the orientations of the yarns in the real woven composites, θ_i, $i = 1, 2, ..., N_\mathrm{s}/2$, for the "V-M" or "LVM" models, are randomly picked in $[70°, 110°]$ following a uniform distribution. For the "VLM" model, θ_i^f and θ_i^g, $i = 1, 2, ..., N_\mathrm{s}/2$, are also randomly picked in respectively $[65°, 115°]$ and $[-15°, 15°]$, following a uniform distribution. It has to be noted that the resulting values of θ_i, θ_i^g and θ_i^f can be out of their initialisation ranges after training, and that this is also the case for the short fibre aspect ratio α_i.

6.3.1. Learning rates

The adopted learning rates for the "V-M" and "LVM" models are

$$\boldsymbol{\eta}^{\mathrm{VM}} = \boldsymbol{\eta}^{\mathrm{LVM}} = \{\eta_v,\, \eta_\theta,\, \eta_\alpha\} = \{0.001,\, 0.01,\, 0.1\}\,, \tag{54}$$

and are, for the "VLM" model,

$$\boldsymbol{\eta}^{\mathrm{VLM}} = \{\eta_v,\, \eta_{\theta\mathrm{g}},\, \eta_{v\mathrm{m}},\, \eta_{\theta\mathrm{f}},\, \eta_\alpha\} = \{0.001,\, 0.01,\, 0.001,\, 0.01,\, 0.1\}\,. \tag{55}$$

A Lagrange multiplier $\lambda = 200$ is used in the loss function, see Eq. (24).

6.3.2. Results

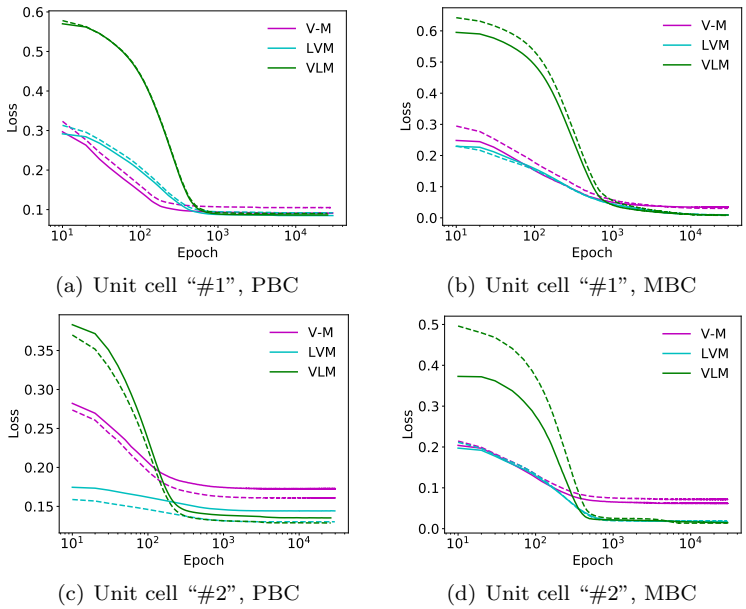

(a) Unit cell "#1", PBC (b) Unit cell "#1", MBC

(c) Unit cell "#2", PBC (d) Unit cell "#2", MBC

Figure 8: Decrease of the loss with the training epochs, "solid" and "dash" lines respectively correspond to the training and testing data.

For both the unit cells "#1" and "#2", 200 samples are generated under each kind of boundary conditions and 20% of the data are used as training data and the remaining 80% as testing data. The decreases of the loss with the training epochs are plotted in Fig. 8 for the two unit cells. It can be seen in Fig. 8 that the decreases of the loss on training and testing data have the same trend with a little divergence, which indicates that the various material properties of the training data have a reduced effect on the learning process of the geometrical parameters $\boldsymbol{\chi}$.

Figure 8 also shows that the "V-M" model and the "VLM" model reach respectively the highest and lowest loss among the three models, and that the "LVM" model is in between. Indeed, because of the model's simpler formulation, the "V-M" model cannot reproduce well the stiffness along the thickness direction (the "z"-direction) of woven unit cells. The "V-M" and "LVM" models can be seen as special cases of the "VLM" model: for $v_1^{\mathrm{g}} = v_0$, $v_1^{\mathrm{m}} = 1.0$ and all the remaining $v_i^{\mathrm{m}} = 0$, $i = 2, ..., N_{\mathrm{s}}$, the "VLM" model reduces to the "V-M" model; and with $\boldsymbol{\theta}_i^{\mathrm{g}} = \mathbf{0}$, and $v_i^{\mathrm{m}} = v_0$, $i = 1, ..., N_{\mathrm{s}}$, the "VLM" model reduces to the "LVM" model. Therefore, it appears that the "VLM" model is more general and flexible than the two other models.

Table 3: Final $\underline{N}_s$ and loss reached after training.

Unit Cell	BCs	Model	$\underline{N}_s$	Loss
"#1"	PBC	V-M	5×2	0.102
		LVM	6×2	0.090
		VLM	7×2	0.089
	MBC	V-M	2×2	0.031
		LVM	8×2	0.010
		VLM	8×2	0.008
"#2"	PBC	V-M	4×2	0.163
		LVM	6×2	0.133
		VLM	8×2	0.130
	MBC	V-M	3×2	0.070
		LVM	10×2	0.019
		VLM	6×2	0.015

The effect of the boundary conditions can also be seen in Fig. 8. On the one hand, the three proposed models can reproduce accurately the homogenised elasticity tensors obtained under MBC, see Figs. 8(b) and 8(d), on the other hand, their predictions for the homogenised elastic tensors obtained under PBC are less accurate, see Figs. 8(a) and 8(c). As discussed in Section 6.2, the reference elasticity tensor obtained under PBC corresponds to a high in-plane Poisson ratio, which indicates a strong coupling between the two in-plane directions. This strong coupling cannot be well captured by the proposed reduced order schemes and the error of the elasticity tensors obtained by reduced order modelling results mainly from the inaccurate coupling of the two in-plane directions.

The training was initialised with $N_s/2 = 40$ short fibre reinforced matrix pseudo-grains for the warp yarn, and the final values of $\underline{N}_s$ reached after 30000 epochs of training and merging are presented in Tab. 3 for the three models, together with the corresponding loss. Since the "VLM" model is the most flexible one among the three models, it accounts for more geometrical information and leads to the most accurate predictions among the three models.

Figure 6 shows that a yarn in the unit cell "#2" has more waviness than in the unit cell "#1". Therefore, it is expected that the woven unit cell "#2" needs more pseudo-grains in the proposed models than the unit cell "#1", which is confirmed by Tab. 3. The coupling in the two in-plane directions is also stronger in unit cell "#2" than in unit cell "#1", which leads to a higher loss for the unit cell "#2" under PBC, independently of the model. The simulation comparisons in the following section will show that the error on the elasticity tensors remains mainly on the coupling in the two in-plane directions.

6.4. Nonlinear analyses

Once the three models have been trained for the two unit cells, they can be used to conduct nonlinear analyses of the woven composites with the real material properties, which are presented in Tab. 4. In particular:

- The matrix phase is modelled as an isotropic elasto-plastic material following J2-plasticity with the hardening law

$$R_0(p) = h_0 \left(1 - e^{-m_0 p}\right) , \tag{56}$$

  where p is the accumulated plastic strain of material, and h_0 and m_0 are the material parameters.

- The typical mechanical properties of Polymerisation of AcryloNitrile (PAN) based high strain carbon fibres are adopted for the transverse isotropic linear elastic fibre.

Table 4: Material properties for the nonlinear analyses [2, 34, 45, 46].

Matrix (8552 epoxy)		Fibre (AS4 carbon fibre)	
Property	Value	Property	Value
Young's modulus E_0 [GPa]	4.668	Young's modulus $E_{\mathrm{I}}^{\mathrm{L}}$ [GPa]	231.0
Poisson ratio ν_0 [-]	0.39	Young's modulus $E_{\mathrm{I}}^{\mathrm{T}}$ [GPa]	12.9
Initial yield stress $\sigma_{\mathrm{Y}0}$ [MPa]	32.0	Poisson ratio $\nu_{\mathrm{I}}^{\mathrm{TT}}$ [-]	0.46
Hardening modulus h_0 [MPa]	150.0	Poisson ratio $\nu_{\mathrm{I}}^{\mathrm{LT}}$ [-]	0.3
Hardening exponent m_0 [-]	300.0	shear modulus $\mu_{\mathrm{I}}^{\mathrm{LT}}$ [GPa]	11.3

6.4.1. Unidirectional tensile test

Direct Numerical Simulations (DNS) were carried out on the two woven unit cells as reference results. The unit cells are subjected to unidirectional tensile loading/unloading along the "x"-direction (weft direction), see Fig. 6, and the applied boundary conditions are successively PBC and MBC. The evolution curves of the macro stress $\sigma_{\mathrm{M}xx}$ with the macro strain $\varepsilon_{\mathrm{M}xx}$ are reported in Figs. 9(a) and 9(b) for the unit cell "#1", and in Figs. 9(c) and 9(d) for the unit cell "#2". In Fig. 9, the boundary conditions applied on the unit cells are indicated by either "PBC" or "MBC" for the direct finite element results.

The three presented models are now considered with their respective geometrical parameters vector $\boldsymbol{\chi}$ obtained considering either PBC or MBC during the training stage. Except for the unit cell "#2" under PBC, see Fig. 9(c), the three presented models capture the macro stress, $\sigma_{\mathrm{M}xx}$, well in comparison to the direct finite element analyses, including during the unloading stage. The predictions of the three models almost overlap each other with little discrepancy. For the more compact unit cell "#2", the rotation of the yarn has an

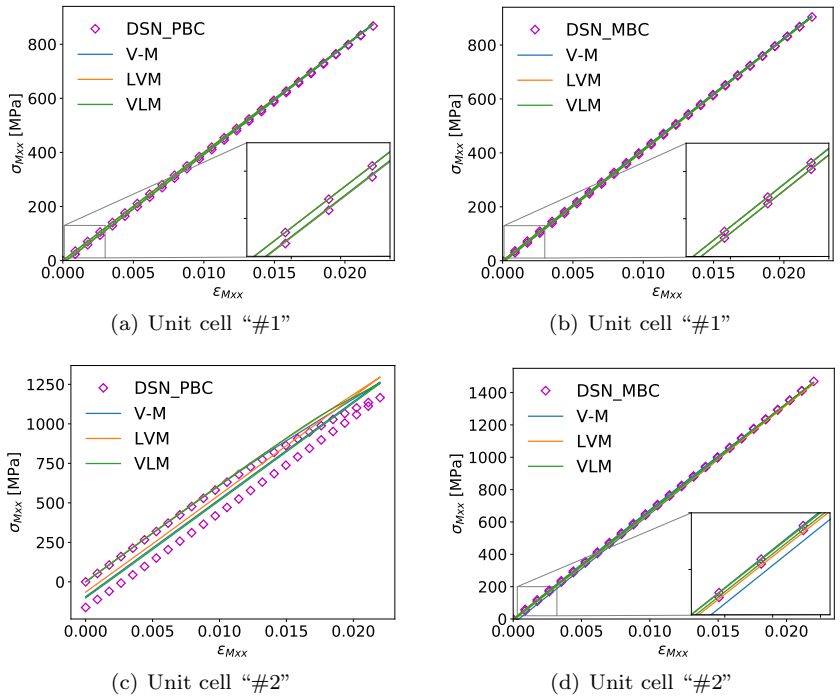

(a) Unit cell "#1"

(b) Unit cell "#1"

(c) Unit cell "#2"

(d) Unit cell "#2"

Figure 9: Unidirectional cyclic tensile tests on the woven unit cells.

obvious impact on the topology of unit cell under PBC, see Fig. 7(a), and this cannot be modelled by the proposed ROMs which assume a negligible change in the cell topology. However, this kind of deformation is more physical when considering woven fabrics than woven composites. Although for a real physical material, the failure of the woven unit cell would have happened before reaching $\varepsilon_{\mathrm{M}xx} = 0.02$, we have considered an applied strain $\varepsilon_{\mathrm{M}xx}$ reaching 0.06 in the tensile tests conducted under MBC, see Fig 10, in order to assess the model accuracy. A discrepancy appears for the unit cell "#2" during the plasticity stage, which is better investigated in shearing in the next section.

6.4.2. In-plane shearing test

The two woven unit cells are now subjected to a in-plane ("x-y" plane) shearing. The loading and constraints are illustrated in Fig. 11. PBC and MBC are successively considered, although the effect of boundary conditions is not distinct in this test.

The reference results of homogenised shear strain-stress curves are obtained by direct numerical simulations and are presented in Fig. 12 for both the PBC and MBC cases. The ROM predictions of the macro-strain, $\varepsilon_{\mathrm{M}xy}$, macro-stress, $\sigma_{\mathrm{M}xy}$, evolution curves are also plotted in Fig. 12(a) for the unit cell "#1" and in Fig. 12(b) for the unit cell "#2". The three ROMs were considered

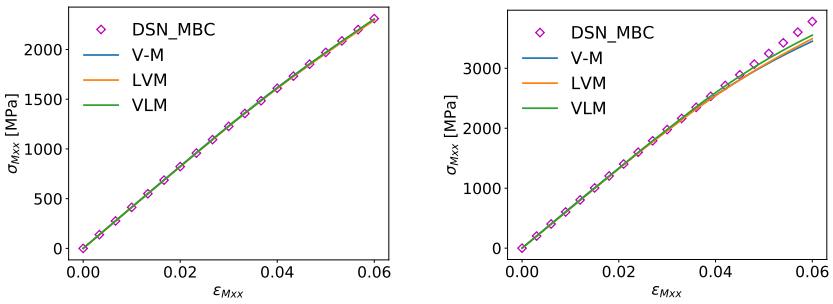

(a) Unit cell #1 (b) Unit cell #2

Figure 10: Unidirectional tensile tests on the woven unit cells under MBC.

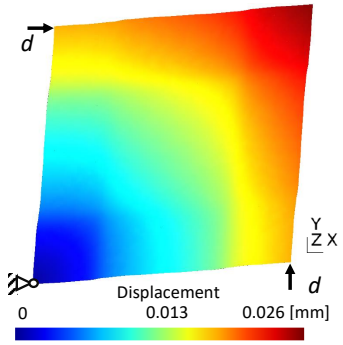

Figure 11: Loading and constraints on a unit cell for the shearing test.

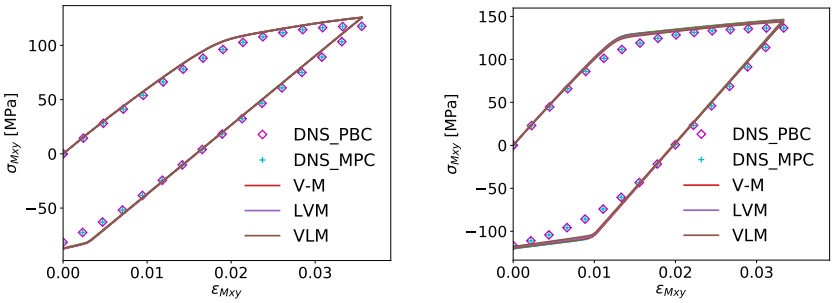

(a) Unit cell #1 (b) Unit cell #2

Figure 12: In-plane cyclic shearing tests on the woven unit cells.

using their respective geometrical parameters $\boldsymbol{\chi}$ identified during the training stage when considering either PBC or MBC and already used for the tensile

Table 5: Computation cost, "Tensile" holds for "unidirectional cyclic tensile test" and "Shear" for "in-plane cyclic shearing test".

-	Unit cell "#1"		Unit cell "#2"	
Model (time steps)	Tensile	Shear	Tensile	Shear
DNS (time steps)	14.5h (500)	81h (1500)	11h (500)	76h (1500)
"V-M" (150)	30s	18s	30s	22s
"LVM" (150)	33s	20s	35s	25s
"VLM" (150)	33s	20s	35s	22s

tests. Therefore, there are totally 6 reduced order modelling curves on each figure, but they overlap on each other for both woven unit cells, see Fig. 12. Good agreements are seen between the results obtained by direct numerical simulations and the ROMs for both unit cells.

6.5. Discussion

Among the three proposed ROMs for woven composites, the "VLM" model can reproduce the elasticity tensor of woven composites with the best accuracy whilst the "V-M" model is less accurate compared to the other two, as shown by the loss in Tab. 3. Besides, because of the way of constructing the ROMs, which fits better a laminate structure, the proposed models reproduce with less accuracy the elasticity tensors of woven composites unit cells submitted to PBC which exhibit more out-of-plane deformation than with MBC, affecting the in-plane Poisson ratio.

The nonlinear tests conducted in Section 6.4 show that the three ROMs provide results with a similar accuracy as compared to direct numerical simulations. In particular, the tensile and shearing tests conducted on unit cells under MBC are well reproduced by the three ROMs. When considering PBC on the unit-cell, the ROMs and the direct numerical simulations agree well in terms of the initial slopes of strain-stress curves, demonstrating that the error seen in the loss results indeed from the in-plane Poisson ratio, which is higher with PBC. However, as discussed in Section 6.2, the MBC on unit cells reflects better the actual state of woven composites than PBC.

The tests performed under MBC are used as examples to compare the computational efficiency of the proposed models. In the direct numerical simulations conducted on the meshes described in Tab. 2, the increment of time step is limited by the small size of the elements and the convergence of the nonlinear analyses, including the MFH scheme used in the yarns. For the direct numerical simulations, 500 time steps are used for the cyclic tensile test and 1500 for the cyclic shearing test. Only 150 time steps are used for the ROMs, and the comparison of the computation costs is presented in Tab. 5. Although the number of degrees of freedom of the cells used in the direct numerical simulations

remains limited, the computational cost of the direct numerical simulations is 3 orders of magnitude higher than with the proposed ROMs.

7. Conclusions

Based on different micro-mechanics models, e.g. mean-field homogenisation and Voigt's rule of mixture, and on the theory of laminate, three ROMs are proposed for woven composites. The ROMs use a bunch of short fibres reinforced matrix material pseudo-grains to model the curved yarn, which is assimilated to a continuous fibre reinforced matrix, in woven composites, completed by pure matrix parts. The main difference of the three models lies in the assumptions adopted for the spatial arrangement of the short fibre reinforced matrix pseudo-grains and the pure matrix material.

A set of homogenised elasticity tensors evaluated by computational homogenisation of woven unit-cells is used as training data in order to identify the topological parameters of the ROMs: for each of the spatial arrangement assumption, a learning process is used to identify the number and parameters of the pseudo-grains by minimising the difference between the homogenised elasticity tensors resulting from the computational homogenisation and ROM predictions.

Equipped with the determined topological parameters, the proposed ROMs can then be applied to conduct nonlinear analyses of woven composites. The accuracy and efficiency of the proposed ROMs have been verified by comparing their predictions with direct numerical simulations on two different woven unit cells. The computation cost is reduced by 3 orders of magnitude with the proposed ROM while accuracy is also guaranteed, in particular when considering that the woven cell deforms using the laminate assumption, i.e. when the top and bottom surfaces do not follow periodic boundary conditions along their out of plane direction but remain planar.

Because of the simple topological parameter definition used in the proposed ROMs, the loading states in the pseudo-grains can be easily linked to the microstructure of the woven unit cells. This can help users to have an intuitive information on the stress state in the studied structure. Although the ROMs are developed for 2D woven composites, the presented methodology can also been applied on 3D woven cases. In the future work, the presented models will be enhanced by adding damage variables in the matrix [40] and fibres [34, 47]. The MFH formula developed in the finite strain regime [48] can also be considered.

Appendix A. Eshelby tensor for an ellipsoidal shape inclusion in an elastic isotropic medium

An ellipsoidal inclusion of prolate shape is defined by its lengths along the principal axes which satisfy $a_1 = a_2 < a_3$. For the aspect ratio $\alpha = a_3/a_1 = a_3/a_2$, the Eshelby tensor $\mathbb{S}$ of this ellipsoidal inclusion in an isotropic matrix

can be expressed in its principal coordinates as shown below,

$$
\begin{aligned}
S_{xxxx} = S_{yyyy} &= \frac{3}{8(1-\nu_0)}(1+\frac{1}{\alpha^2-1}) + \frac{1}{4(1-\nu_0)}\left[1-2\nu_0-\frac{9}{4(\alpha^2-1)}\right]g \\
S_{zzzz} &= \frac{1}{2(1-\nu_0)}\left\{4-2\nu_0+\frac{2}{\alpha^2-1}-\left[4-2\nu_0+\frac{3}{\alpha^2-1}\right]g\right\} \\
S_{xxyy} = S_{yyxx} &= \frac{1}{4(1-\nu_0)}\left\{\frac{1}{2}+\frac{1}{2(\alpha^2-1)}-\left[1-2\nu_0+\frac{3}{4(\alpha^2-1)}\right]g\right\} \\
S_{xxzz} = S_{yyzz} &= -\frac{1}{2(1-\nu_0)}\left(1+\frac{1}{\alpha^2-1}\right)+\frac{1}{4(1-\nu_0)}\left[3+\frac{3}{\alpha^2-1}-(1-2\nu_0)\right]g \\
S_{zzxx} = S_{zzyy} &= -\frac{1}{2(1-\nu_0)}\left[1-2\nu_0+\frac{1}{\alpha^2-1}\right]+\frac{1}{2(1-\nu_0)}\left[1-2\nu_0+\frac{3}{2(\alpha^2-1)}\right]g \\
S_{xyxy} &= \frac{1}{4(1-\nu_0)}\left\{\frac{1}{2}+\frac{1}{2(\alpha^2-1)}+\left[1-2\nu_0-\frac{3}{4(\alpha^2-1)}\right]g\right\} \\
S_{xzxz} = S_{yzyz} &= \frac{1}{4(1-\nu_0)}\left\{-2\nu_0-\frac{2}{\alpha^2-1}-\frac{1}{2}\left[-2-2\nu_0-\frac{6}{\alpha^2-1}\right]g\right\}, \qquad \text{(A.1)}
\end{aligned}
$$

where ν_0 is the Poisson ratio of the matrix, and

$$
g = \frac{\alpha}{(\alpha^2-1)^{3/2}}\left[\alpha(\alpha^2-1)^{1/2}-\cosh^{-1}\alpha\right]. \qquad \text{(A.2)}
$$

The other components of $\mathbb{S}$ can be obtained using the minor symmetry condition, $S_{ijkl} = S_{jikl} = S_{ijlk}$.

Appendix B. Evaluation of the gradient $\boldsymbol{\nabla L(\chi)}$

Appendix B.1. For the "V-M" model

According to the computation process of $\mathbb{C}^{\mathrm{VM}}$ reported in Section 3.1, one has

$$
\begin{aligned}
\frac{\partial L}{\partial v_i} &= \frac{\partial L}{\partial \mathbb{C}^{\mathrm{VM}}} :: \frac{\partial \mathbb{C}^{\mathrm{VM}}}{\partial v_i} + \frac{\lambda}{2}\frac{\partial G}{\partial v_i}, \qquad \text{(B.1)} \\
\frac{\partial L}{\partial \alpha_i} &= \frac{\partial L}{\partial \mathbb{C}^{\mathrm{VM}}} :: \frac{\partial \mathbb{C}^{\mathrm{VM}}}{\partial \mathbb{C}_i} :: \frac{\partial \mathbb{C}_i}{\partial \mathbb{S}_i} :: \frac{\partial \mathbb{S}_i}{\partial \alpha_i}, \qquad \text{(B.2)} \\
\left[\frac{\partial L}{\partial \boldsymbol{\theta}_i}\right]_k &= \frac{\partial L}{\partial \mathbb{C}^{\mathrm{VM}}} :: \frac{\partial \mathbb{C}^{\mathrm{VM}}}{\partial \mathbb{R}(\boldsymbol{\theta}_i)} :: \frac{\partial \mathbb{R}(\boldsymbol{\theta}_i)}{\partial \theta_i^k}, \qquad \text{(B.3)}
\end{aligned}
$$

where $i = 1, 2, ..., N_{\mathrm{s}}$, where the Eshelby tensor $\mathbb{S}_i = \mathbb{S}(\mathrm{I}_i, \mathbb{C}_0)$ is given in Appendix A, and where $k = 1, 2, 3$ is the index for the elements of $\boldsymbol{\theta}_i = [\theta_i^1, \theta_i^2, \theta_i^3]$, the three Euler angles defining the orientation.

Appendix B.2. For the "LVM" model

According to the computation process of $\mathbb{C}^{\mathrm{LVM}}$ reported in Section 3.2, one has

$$\frac{\partial L}{\partial v_i} = \frac{\partial L}{\partial \mathbb{C}^{\mathrm{LVM}}} :: \frac{\partial \mathbb{C}^{\mathrm{LVM}}}{\partial \mathbb{C}_{\mathrm{A}}} :: \frac{\partial \mathbb{C}_{\mathrm{A}}}{\partial v_i} + \frac{\lambda}{2}\frac{\partial G}{\partial v_i}\,, \tag{B.4}$$

$$\frac{\partial L}{\partial \alpha_i} = \frac{\partial L}{\partial \mathbb{C}^{\mathrm{LVM}}} :: \frac{\partial \mathbb{C}^{\mathrm{LVM}}}{\partial \mathbb{C}_{\mathrm{A}}} :: \frac{\partial \mathbb{C}_{\mathrm{A}}}{\partial \mathbb{C}_i} :: \frac{\partial \mathbb{C}_i}{\partial \mathbb{S}_i} :: \frac{\partial \mathbb{S}_i}{\partial \alpha_i}\,, \tag{B.5}$$

$$\left[\frac{\partial L}{\partial \boldsymbol{\theta}_i}\right]_k = \frac{\partial L}{\partial \mathbb{C}^{\mathrm{LVM}}} :: \frac{\partial \mathbb{C}^{\mathrm{LVM}}}{\partial \mathbb{C}_{\mathrm{A}}} :: \frac{\partial \mathbb{C}_{\mathrm{A}}}{\partial \mathbb{R}(\boldsymbol{\theta}_i)} :: \frac{\partial \mathbb{R}(\boldsymbol{\theta}_i)}{\partial \theta_i^k}\,, \tag{B.6}$$

where $i = 1,\, 2, ..., N_{\mathrm{s}}$.

Appendix B.3. For the "VLM" model

According to the computation process of $\mathbb{C}^{\mathrm{VLM}}$ reported in Section 3.3, one has

$$\frac{\partial L}{\partial v_i^{\mathrm{g}}} = \frac{\partial L}{\partial \mathbb{C}^{\mathrm{VLM}}} :: \frac{\partial \mathbb{C}^{\mathrm{VLM}}}{\partial v_i^{\mathrm{g}}} + \frac{\lambda}{2}\frac{\partial G}{\partial v_i^{\mathrm{g}}}\,, \tag{B.7}$$

$$\left[\frac{\partial L}{\partial \boldsymbol{\theta}_i^{\mathrm{g}}}\right]_k = \frac{\partial L}{\partial \mathbb{C}^{\mathrm{VLM}}} :: \frac{\partial \mathbb{C}^{\mathrm{VLM}}}{\partial \mathbb{R}(\boldsymbol{\theta}_i^{\mathrm{g}})} :: \frac{\partial \mathbb{R}(\boldsymbol{\theta}_i^{\mathrm{g}})}{\partial \theta_i^{\mathrm{g},k}}\,, \tag{B.8}$$

$$\frac{\partial L}{\partial \alpha_i} = \frac{\partial L}{\partial \mathbb{C}^{\mathrm{VLM}}} :: \frac{\partial \mathbb{C}^{\mathrm{VLM}}}{\partial \mathbb{C}_{\mathrm{L}i}} :: \frac{\partial \mathbb{C}_{\mathrm{L}i}}{\partial \mathbb{C}_{\mathrm{A}i}} : \frac{\partial \mathbb{C}_{\mathrm{A}i}}{\partial \mathbb{C}_i} :: \frac{\partial \mathbb{C}_i}{\partial \mathbb{S}_i} :: \frac{\partial \mathbb{S}_i}{\partial \alpha_i}\,, \tag{B.9}$$

$$\frac{\partial L}{\partial v_i^{\mathrm{m}}} = \frac{\partial L}{\partial \mathbb{C}^{\mathrm{VLM}}} :: \frac{\partial \mathbb{C}^{\mathrm{VLM}}}{\partial \mathbb{C}_{\mathrm{L}i}} :: \frac{\partial \mathbb{C}_{\mathrm{L}i}}{\partial v_i^{\mathrm{m}}} + \frac{\lambda}{2}\frac{\partial G}{\partial v_i^{\mathrm{m}}}\,, \tag{B.10}$$

$$\left[\frac{\partial L}{\partial \boldsymbol{\theta}_i^{\mathrm{f}}}\right]_l = \frac{\partial L}{\partial \mathbb{C}^{\mathrm{VLM}}} :: \frac{\partial \mathbb{C}^{\mathrm{VLM}}}{\partial \mathbb{C}_{\mathrm{L}i}} :: \frac{\partial \mathbb{C}_{\mathrm{L}i}}{\partial \mathbb{C}_{\mathrm{A}i}} :: \frac{\partial \mathbb{C}_{\mathrm{A}i}}{\partial \mathbb{R}(\boldsymbol{\theta}_i^{\mathrm{f}})} :: \frac{\partial \mathbb{R}(\boldsymbol{\theta}_i^{\mathrm{f}})}{\partial \theta_i^{\mathrm{f},l}}\,, \tag{B.11}$$

where $i = 1,\, 2, ..., N_{\mathrm{s}}$, and where $k, l = 1, 2, 3$ are indexes for the elements of the Euler angles vectors $\boldsymbol{\theta}_i^{\mathrm{g}} = [\theta_i^{\mathrm{g},1},\, \theta_i^{\mathrm{g},2},\, \theta_i^{\mathrm{g},3}]$ and $\boldsymbol{\theta}_i^{\mathrm{f}} = [\theta_i^{\mathrm{f},1},\, \theta_i^{\mathrm{f},2},\, \theta_i^{\mathrm{f},3}]$, respectively.

Appendix B.4. Rotation tensor

Euler angles $(z - x' - z'')$ are adopted, and only the orientation of the fibre in the warp yarn needs to be considered according to the dimension reduction of Section 6.1. Therefore, all the considered Euler angles $\boldsymbol{\theta}_i$, $\boldsymbol{\theta}_i^{\mathrm{g}}$ and $\boldsymbol{\theta}_i^{\mathrm{f}}$ can be reduced to respectively $[0, \theta_i, 0]$, $[0, \theta_i^{\mathrm{g}}, 0]$ and $[0, \theta_i^{\mathrm{f}}, 0]$. Considering in the Voigt's notations that the stress tensor and the strain tensor are respectively represented by $\boldsymbol{\sigma} = [\sigma_{xx}\ \ \sigma_{yy}\ \ \sigma_{zz}\ \ \sqrt{2}\sigma_{xy}\ \ \sqrt{2}\sigma_{xz}\ \ \sqrt{2}\sigma_{yz}]^T$ and

$\boldsymbol{\varepsilon} = [\varepsilon_{xx}\ \varepsilon_{yy}\ \varepsilon_{zz}\ \sqrt{2}\varepsilon_{xy}\ \sqrt{2}\varepsilon_{xz}\ \sqrt{2}\varepsilon_{yz}]^T$ and the material tensor by

$$\mathbb{C} = \begin{bmatrix} C_{xxxx} & C_{xxyy} & C_{xxzz} & \sqrt{2}C_{xxxy} & \sqrt{2}C_{xxxz} & \sqrt{2}C_{xxyz} \\ C_{xxyy} & C_{yyyy} & C_{yyzz} & \sqrt{2}C_{yyxy} & \sqrt{2}C_{yyxz} & \sqrt{2}C_{yyyz} \\ C_{xxzz} & C_{yyzz} & C_{zzzz} & \sqrt{2}C_{zzxy} & \sqrt{2}C_{zzxz} & \sqrt{2}C_{zzyz} \\ \sqrt{2}C_{xyxx} & \sqrt{2}C_{xyyy} & \sqrt{2}C_{xyzz} & 2C_{xyxy} & 2C_{xyxz} & 2C_{xyyz} \\ \sqrt{2}C_{xzxx} & \sqrt{2}C_{xzyy} & \sqrt{2}C_{xzzz} & 2C_{xzxy} & 2C_{xzxz} & 2C_{xzyz} \\ \sqrt{2}C_{yzxx} & \sqrt{2}C_{yzyy} & \sqrt{2}C_{yzzz} & 2C_{yzxy} & 2C_{yzxz} & 2C_{yzyz} \end{bmatrix}, \tag{B.12}$$

then the rotation tensor $\mathbb{R}(\boldsymbol{\theta}_i)$, in its Voigt's notation, reads

$$\boldsymbol{R}([0,\theta,0]) = \begin{bmatrix} 1 & 0 & 0 & 0 & 0 & 0 \\ 0 & \cos^2\theta & \sin^2\theta & \sqrt{2}\cos\theta\sin\theta & 0 & 0 \\ 0 & \sin^2\theta & \cos^2\theta & -\sqrt{2}\cos\theta\sin\theta & 0 & 0 \\ 0 & -\sqrt{2}\cos\theta\sin\theta & \sqrt{2}\cos\theta\sin\theta & \cos^2\theta - \sin^2\theta & 0 & 0 \\ 0 & 0 & 0 & 0 & \cos\theta & -\sin\theta \\ 0 & 0 & 0 & 0 & \sin\theta & \cos\theta \end{bmatrix}, \tag{B.13}$$

which yields

$$\frac{\mathrm{d}\boldsymbol{R}([0,\theta,0])}{\mathrm{d}\theta} = \begin{bmatrix} 0 & 0 & 0 & 0 & 0 & 0 \\ 0 & -2\cos\theta\sin\theta & 2\cos\theta\sin\theta & \sqrt{2}(\cos^2\theta - \sin^2\theta) & 0 & 0 \\ 0 & 2\cos\theta\sin\theta & -2\cos\theta\sin\theta & \sqrt{2}(\sin^2\theta - \cos^2\theta) & 0 & 0 \\ 0 & \sqrt{2}(\sin^2\theta - \cos^2\theta) & \sqrt{2}(\cos^2\theta - \sin^2\theta) & -4\cos\theta\sin\theta & 0 & 0 \\ 0 & 0 & 0 & 0 & -\sin\theta & -\cos\theta \\ 0 & 0 & 0 & 0 & \cos\theta & -\sin\theta \end{bmatrix}. \tag{B.14}$$

Acknowledgment

The research has been funded by the Walloon Region under the agreement n^o.7911-VISCOS in the context of the 21st SKYWIN call.

Data availability

The raw/processed data required to reproduce these findings is available on [49] under the Creative Commons Attribution 4.0 International (CC BY 4.0) licence.

[1] T. Ishikawa, T. W. Chou, Stiffness and strength behaviour of woven fabric composites, Journal of Materials Science 17 (1982) 3211–3220, doi: https://doi.org/10.1007/BF01203485.

[2] HexTow © AS4, Carbon Fiber, Product Data Sheet, Hexcel Corporation, 2018.

[3] W. R. Yu, F. Pourboghrat, K. Chung, M. Zampaloni, T. J. Kang, Non-orthogonal constitutive equation for woven fabric reinforced thermoplastic composites, Composites Part A: Applied Science and Manufacturing 33 (8) (2002) 1095 – 1105, ISSN 1359-835X, doi:https://doi.org/10.1016/S1359-835X(02)00053-2.

[4] X. Peng, J. Cao, A continuum mechanics-based non-orthogonal constitutive model for woven composite fabrics, Composites Part A: Applied Science and Manufacturing 36 (6) (2005) 859 – 874, ISSN 1359-835X, doi:https://doi.org/10.1016/j.compositesa.2004.08.008.

[5] M. King, P. Jearanaisilawong, S. Socrate, A continuum constitutive model for the mechanical behavior of woven fabrics, International Journal of Solids and Structures 42 (13) (2005) 3867 – 3896, ISSN 0020-7683, doi:https://doi.org/10.1016/j.ijsolstr.2004.10.030.

[6] M. G. D. Geers, V. G. Kouznetsova, W. A. M. Brekelmans, Multi-scale computational homogenization: Trends and challenges, Journal of Computational and Applied Mathematics 234 (7) (2010) 2175–2182, ISSN 0377-0427, doi:DOI: 10.1016/j.cam.2009.08.077, fourth International Conference on Advanced COmputational Methods in ENgineering (ACOMEN 2008).

[7] L. Noels, L. Wu, L. Adam, J. Seyfarth, G. Soni, J. Segurado, G. Laschet, G. Chen, M. Lesueur, M. Lobos, T. Bhlke, T. Reiter, S. Oberpeilsteiner, D. Salaberger, D. Weichert, C. Broeckmann, Effective Properties, chap. 6, John Wiley & Sons, Ltd, ISBN 9783527693566, 433–485, doi:10.1002/9783527693566.ch6, URL https://onlinelibrary.wiley.com/doi/abs/10.1002/9783527693566.ch6, 2016.

[8] S. V. Lomov, D. S. Ivanov, I. Verpoest, M. Zako, T. Kurashiki, H. Nakai, S. Hirosawa, Meso-FE modelling of textile composites: Road map, data flow and algorithms, Composites Science and Technology 67 (9) (2007) 1870 – 1891, ISSN 0266-3538, doi:https://doi.org/10.1016/j.compscitech.2006.10.017.

[9] N. De Carvalho, S. Pinho, P. Robinson, Reducing the domain in the mechanical analysis of periodic structures, with application to woven composites, Composites Science and Technology 71 (7) (2011) 969 – 979, ISSN 0266-3538, doi:https://doi.org/10.1016/j.compscitech.2011.03.001, URL http://www.sciencedirect.com/science/article/pii/S0266353811000911.

[10] C. M. Pastore, A. E. Bogdanovich, Y. A. Gowayed, Applications of a meso-volume-based analysis for textile composite structures, Composites Engineering 3 (2) (1993) 181 – 194, ISSN 0961-9526, doi:https://doi.org/10.1016/0961-9526(93)90041-H, URL http://www.sciencedirect.com/science/article/pii/096195269390041H.

[11] D. S. Ivanov, S. V. Lomov, 2 - Modeling of 2D and 3D woven composites, in: P. Irving, C. Soutis (Eds.), Polymer Composites in the Aerospace Industry (Second Edition), Woodhead Publishing Series in Composites Science and Engineering, Woodhead Publishing, second edition edn., ISBN 978-0-08-102679-3, 23 – 57, doi:https://doi.org/10.1016/B978-0-08-102679-3.00002-2, URL http://www.sciencedirect.com/science/article/pii/B9780081026793000022, 2020.

[12] DIGIMAT, The nonlinear multiscale material modeling platform, URL e-xstream.com, 2021.

[13] N. Bakhvalov, G. Panasenko, Homogenisation: Averaging Processes in Periodic Media, vol. 36 of *Mathematics and its Applications*, Springer, 1 edn., 1989.

[14] J. Fish, Q. Yu, Two-scale damage modeling of brittle composites, Composites Science and Technology 61 (15) (2001) 2215 – 2222, ISSN 0266-3538, doi:https://doi.org/10.1016/S0266-3538(01)00115-4, URL http://www.sciencedirect.com/science/article/pii/S0266353801001154.

[15] R. Hill, A self-consistent mechanics of composite materials, Journal of the Mechanics and Physics of Solids 13 (4) (1965) 213 – 222, ISSN 0022-5096, doi:DOI: 10.1016/0022-5096(65)90010-4.

[16] X. Han, J. Gao, M. Fleming, C. Xu, W. Xie, S. Meng, W. K. Liu, Efficient multiscale modeling for woven composites based on self-consistent clustering analysis, Computer Methods in Applied Mechanics and Engineering 364 (2020) 112929, ISSN 0045-7825, doi:https://doi.org/10.1016/j.cma.2020.112929, URL http://www.sciencedirect.com/science/article/pii/S0045782520301122.

[17] T. Mori, K. Tanaka, Average stress in matrix and average elastic energy of materials with misfitting inclusions, Acta Metallurgica 21 (5) (1973) 571–574, cited By (since 1996) 1814.

[18] L. Wu, V. D. Nguyen, N. G. Kilingar, L. Noels, A recurrent neural network-accelerated multi-scale model for elasto-plastic heterogeneous materials subjected to random cyclic and non-proportional loading paths, Computer Methods in Applied Mechanics and Engineering 369 (2020) 113234, ISSN 0045-7825, doi:https://doi.org/10.1016/j.cma.2020.113234, URL https://www.sciencedirect.com/science/article/pii/S0045782520304199.

[19] H. J. Logarzo, G. Capuano, J. J. Rimoli, Smart constitutive laws: Inelastic homogenization through machine learning, Computer Methods in Applied Mechanics and Engineering 373 (2021) 113482, ISSN 0045-7825, doi:https://doi.org/10.1016/j.cma.2020.113482, URL https://www.sciencedirect.com/science/article/pii/S0045782520306678.

[20] R. Xu, J. Yang, W. Yan, Q. Huang, G. Giunta, S. Belouettar, H. Zahrouni, T. Ben Zineb, H. Hu, Data-driven multiscale finite element method: From concurrence to separation, Computer Methods in Applied Mechanics and Engineering 363 (2020) 112893, ISSN 0045-7825, doi:https://doi.org/10.1016/j.cma.2020.112893, URL https://www.sciencedirect.com/science/article/pii/S004578252030075X.

[21] T. Kirchdoerfer, M. Ortiz, Data-driven computational mechanics, Computer Methods in Applied Mechanics and Engineering 304 (2016) 81–101, ISSN 0045-7825, doi:https://doi.org/10.1016/j.cma.2016.02.001, URL https://www.sciencedirect.com/science/article/pii/S0045782516300238.

[22] R. Eggersmann, T. Kirchdoerfer, S. Reese, L. Stainier, M. Ortiz, Model-Free Data-Driven inelasticity, Computer Methods in Applied Mechanics and Engineering 350 (2019) 81–99, ISSN 0045-7825, doi:https://doi.org/10.1016/j.cma.2019.02.016, URL https://www.sciencedirect.com/science/article/pii/S0045782519300878.

[23] M. Bessa, R. Bostanabad, Z. Liu, A. Hu, D. W. Apley, C. Brinson, W. Chen, W. K. Liu, A framework for data-driven analysis of materials under uncertainty: Countering the curse of dimensionality, Computer Methods in Applied Mechanics and Engineering 320 (2017) 633–667, ISSN 0045-7825, doi:https://doi.org/10.1016/j.cma.2017.03.037, URL https://www.sciencedirect.com/science/article/pii/S0045782516314803.

[24] Z. Liu, C. Wu, M. Koishi, A deep material network for multiscale topology learning and accelerated nonlinear modeling of heterogeneous materials, Computer Methods in Applied Mechanics and Engineering 345 (2019) 1138 – 1168, ISSN 0045-7825, doi:https://doi.org/10.1016/j.cma.2018.09.020.

[25] Z. Liu, C. Wu, Exploring the 3D architectures of deep material network in data-driven multiscale mechanics, Journal of the Mechanics and Physics of Solids 127 (2019) 20 – 46, ISSN 0022-5096, doi:https://doi.org/10.1016/j.jmps.2019.03.004, URL http://www.sciencedirect.com/science/article/pii/S0022509618310688.

[26] S. Gajek, M. Schneider, T. Böhlke, On the micromechanics of deep material networks, Journal of the Mechanics and Physics of Solids 142 (2020) 103984, ISSN 0022-5096, doi:10.1016/j.jmps.2020.103984.

[27] V.-D. Nguyen, L. Noels, Micromechanics-based material networks revisited from the interaction viewpoint; robust and efficient implementation for multi-phase composites, European Journal of Mechanics - A/Solids .

[28] R. Hill, The Elastic Behaviour of a Crystalline Aggregate, Proceedings of the Physical Society. Section A 65 (5) (1952) 349–354, doi:10.1088/0370-1298/65/5/307.

[29] W. Voigt, Über die Beziehung zwischen den beiden Elastizitätskonstanten isotroper Körper, Wied Ann 38 (1889) 573 – 587.

[30] I. Doghri, L. Tinel, Micromechanical modeling and computation of elasto-plastic materials reinforced with distributed-orientation fibers, International Journal of Plasticity 21 (10) (2005) 1919 – 1940, ISSN 0749-6419, doi:10.1016/j.ijplas.2004.09.003.

[31] J. Segurado, J. Llorca, A numerical approximation to the elastic properties of sphere-reinforced composites, Journal of the Mechanics and Physics of Solids 50 (10) (2002) 2107 – 2121, ISSN 0022-5096.

[32] T. Kurashiki, M. Zako, S. Hirosawa, S. Lomov, I. Verpoest, Estimation of a mechanical characterization for woven fabric composites by fem based on damage mechanics, in: Materials Science, 2004.

[33] J. D. Eshelby, The Determination of the Elastic Field of an Ellipsoidal Inclusion, and Related Problems, Proceedings of the Royal Society of London. Series A, Mathematical and Physical Sciences 241 (1226) (1957) pp. 376–396, ISSN 00804630.

[34] L. Wu, T. Zhang, E. Maillard, L. Adam, P. Martiny, L. Noels, Per-phase spatial correlated damage models of UD fibre reinforced composites using mean-field homogenisation; application to model the yarn failure of plain woven composites, Computer & Structures .

[35] D. P. Kingma, J. Ba, Adam: A Method for Stochastic Optimization, 2017.

[36] D. R. S. Talbot, J. R. Willis, Bounds and Self-Consistent Estimates for the Overall Properties of Nonlinear Composites, IMA Journal of Applied Mathematics 39 (3) (1987) 215–240.

[37] P. Ponte Castañeda, The effective mechanical properties of nonlinear isotropic composites, Journal of the Mechanics and Physics of Solids 39 (1) (1991) 45–71, ISSN 0022-5096, doi:DOI: 10.1016/0022-5096(91)90030-R.

[38] L. Wu, L. Noels, L. Adam, I. Doghri, A combined incremental-secant mean-field homogenization scheme with per-phase residual strains for elasto-plastic composites, International Journal of Plasticity 51 (2013) 80 – 102, ISSN 0749-6419, doi:https://doi.org/10.1016/j.ijplas.2013.06.006, URL http://www.sciencedirect.com/science/article/pii/S0749641913001174.

[39] L. Wu, I. Doghri, L. Noels, An incremental-secant mean-field homogenization method with second statistical moments for elasto-plastic composite materials, Philosophical Magazine 95 (28-30) (2015) 3348–3384, doi: 10.1080/14786435.2015.1087653.

[40] L. Wu, L. Noels, L. Adam, I. Doghri, An implicit-gradient-enhanced incremental-secant mean-field homogenization scheme for elasto-plastic composites with damage, International Journal of Solids and Structures 50 (24) (2013) 3843 – 3860, ISSN 0020-7683.

[41] L. Wu, L. Noels, L. Adam, I. Doghri, Multiscale mean-field homogenization method for fiber-reinforced composites with gradient-enhanced damage model, Computer Methods in Applied Mechanics and Engineering 233-236 (2012) 164–179, doi:10.1016/j.cma.2012.04.011.

[42] J. Hou, C. Ruiz, Measurement of the properties of woven CFRP T300/914 at different strain rates, Composites Science and Technology 60 (15) (2000) 2829 – 2834, ISSN 0266-3538, doi:https://doi.org/10.1016/S0266-3538(00)00151-2, URL http://www.sciencedirect.com/science/article/pii/S0266353800001512.

[43] H. Sun, N. Pan, R. Postle, On the Poisson's ratios of a woven fabric, Composite Structures 68 (4) (2005) 505 – 510, ISSN 0263-8223, doi:https://doi.org/10.1016/j.compstruct.2004.05.017, URL http://www.sciencedirect.com/science/article/pii/S0263822304001898.

[44] L. Bao, M. Takatera, A. Shinohara, Error Evaluation on Measuring the Apparent Poisson's Ratios of Textile Fabrics by Uniaxial Tensile Test, Sen'i Gakkaishi 53 (1) (1997) 20–26, doi:10.2115/fiber.53.20.

[45] HexPly © 8552, Epoxy matrix (180°C/356°F curing matrix), Product Data Sheet, Hexcel Corporation, 2016.

[46] M. Herráez, A. Fernández, C. S. Lopes, C. González, Strength and toughness of structural fibres for composite material reinforcement, Philos Trans A Math Phys Eng Sci. 374 (2071) (2016) 1–11, ISSN 1471-2962, doi: https://doi.org/10.1098/rsta.2015.0274.

[47] L. Wu, E. Maillard, L. Noels, Tensile failure model of carbon fibre in unidirectionally reinforced epoxy composites with mean-field homogenisation, Composite Structures .

[48] M. El Ghezal, L. Wu, L. Noels, I. Doghri, A finite strain incremental-secant homogenization model for elasto-plastic composites, Computer Methods in Applied Mechanics and Engineering 347 (2019) 754 – 781, ISSN 0045-7825, doi:https://doi.org/10.1016/j.cma.2018.12.007, URL http://www.sciencedirect.com/science/article/pii/S0045782518306054.

[49] L. Wu, L. Adam, L. Noels, Data of "Micro-mechanics and data-driven based reduced order models for multi-scale analyses of woven composites", doi:10.5281/zenodo.4718641, URL https://doi.org/10.5281/zenodo.4718641, The research has been funded by the Walloon Region under the agreement no.7911-VISCOS in the context of the 21st SKYWIN call., 2021.